Structural Control of Fluvial Network Morphology on Titan

A Thesis Presented for the
Master of Science
Degree
The University of Tennessee, Knoxville

Sarah Alice Drummond
August 2012

DEDICATION

This work is dedicated to Suzanne Mericle Hazel, who first inspired my love of planetary science.

ACKNOWLEDGEMENTS

I would first and foremost like to thank my current committee: Devon Burr, Josh Emery, and Bob Hatcher for assistance with interpreting and presenting the results of my research in this thesis. I appreciate the technical support from Trent Hare, Jeff Jenness, and James Rounce. Thanks are also due to all members of previous versions of my committee: Jeff Moersch, Linda Kah, and John Schwartz for kindly offering their time and expertise.

I greatly appreciate the support of my fellow UTK graduate students in the EPS department, as well as planetary science graduate students at other schools who have been sources of encouragement. I also have a great appreciation for the friendship I received from EPS undergraduate students while taking remedial coursework during my first year of graduate school.

I would like to thank my parents and brother, Ned, the Hines family, and my three closest friends and Alpha Delta Pi sisters: Liz Zipperle, Elisabeth Culkowski, and Sammi Kline, for all the love they have given me always, but especially the last three years. Lastly, I would like to acknowledge Yo Matsubara who first encouraged me to get involved in planetary research and has continued to be an excellent mentor and even better friend; and my undergraduate advisor, Alan Howard, who gave me my academic foundation and continues to be a wonderful advisor.

ABSTRACT

Titan fluvial networks have been classed based on identification of network pattern morphology. Drainage network patterns have specific geologic implications, as the pattern is affected by regional slope, structures, and bedrock resistance. Qualitative identification of network patterns has resulted in a lack of consistent classifications for networks. In this work, a global map of fluvial features on Titan is presented with features delineated based on their appearance in Cassini Titan Radar Mapper synthetic aperture radar (SAR) data. The networks imaged by the Huygens Descent Imager/Spectral Radiometer (DISR) are also included in this work. Networks were classified using a quantitative terrestrial drainage pattern classification algorithm modified for use for Titan. This drainage pattern analysis, performed on the 48 networks of 10 or more links imaged in SAR data, results in 56% rectangular networks, 25% dendritic networks, 8% parallel networks, and 10% unclassified networks. All of the 5 networks imaged in DISR are classified as rectangular. This result is inconsistent with the results of previous network pattern identifications that indicated that the majority of networks have a dendritic pattern. Because rectangular networks imply control by joints or faults that intersect at near right angles, the predominance and distribution of rectangular networks suggests that Titan's crust is widely fractured or faulted. A review of terrestrial river networks also classified as rectangular by the same algorithm indicates that tensional stress formed the joints and/or faults controlling the rivers. Based on the similar response of rock and ice to stress, it is inferred that the joints and/or faults controlling rectangular networks on Titan also formed in a tensional tectonic regime. Most of the Titan rectangular networks occur at the north and south poles, indicating that

these areas have undergone regional extension. Rectangular networks are also located in Xanadu, but because of the unique geologic history of this region, those networks are not considered in comparison with the published results of global stress mechanisms. This comparison suggests that regional extension in these locations is not consistent with the stress regimes expected from non-synchronous rotation and polar wander and is more consistent with stress regimes expected from despinning or orbital recession.

TABLE OF CONTENTS

LIST OF TABLES

LIST OF FIGURES

I. INTRODUCTION

Like Earth, Titan has a thick, nitrogen-rich atmosphere that participates in an active volatile cycle and produces a range of surface modifying processes. Clouds of methane, which constitute ~5% of Titan's troposphere, have been observed to form and dissipate over various regions of Titan, implying rainfall (e.g., Griffith *et al.* 2000, Porco *et al.* 2005, Lunine and Atreya, 2008, Atreya *et al.* 2009, Turtle *et al.* 2011). Rain has also been inferred from *in situ* observations near Titan's equator (Tomasko *et al.* 2005). As a result of this precipitation and surface runoff of liquid methane, fluvial networks, thought to be carved into the water ice bedrock (Collins 2005, Perron *et al.* 2006) and/or formed by flow across radar-dark, smooth plains, are widely distributed (Barnes *et al.* 2007, Jaumann *et al.* 2008, Lorenz *et al.* 2008, Baugh 2008, Jaumann *et al.* 2009, Burr *et al.* 2009, Le Gall *et al.* 2010, Cartwright *et al.* 2011, Langhans *et al.* 2012).

Fluvial flow resulting from sapping by subsurface liquid has been suggested to have operated on small networks with stubby tributaries in the northeast wall of Menrva crater (Baugh 2008) and at the Huygens landing site (Tomasko *et al.* 2005), although terrestrial analog work implicates the strong role of overland flow in forming such networks (Lamb *et al.* 2006, 2008). In the polar regions of Titan, the fluvial networks commonly empty into lakes potentially filled with liquid hydrocarbons and nitrogen (Stofan *et al.* 2007, Mitri *et al.* 2007, Hayes *et al.* 2010). Inequatorial regions, dark dune fields provide evidence that aeolian processes are also an active resurfacing agent (Barnes *et al.* 2008, Radebaugh *et al.* 2008). These atmospheric, fluvial, lacustrine, and aeolian features attest to the recent or on-going exogenic modification of Titan's surface. That this activity was recent or is on-going is supported by Titan's low crater density (Lorenz *et al.* 2007, Wall *et al.* 2009, Wood *et al.* 2010, Neish and Lorenz 2012).

For the purposes of this work external processes are defined as those for which the energy for surface modification is supplied externally to the planet's surface. These processes include fluvial and aeolian processes, mass wasting, and impacts. Large equatorial aeolian dune fields attest to recent or on-going aeolian processes (Barnes *et al.* 2008, Radebaugh *et al.* 2008), surface albedo changes after storms indicate precipitation, ponding, and evaporation of methane (Turtle *et al.* 2009, Turtle *et al.* 2011), changes in lake shorelines (Turtle *et al.* 2011) and the albedo (Turtle *et al.* 2009) and radar backscatter of lakes (Hayes *et al.* 2011, Welivitya *et al.* 2012) suggest active lacustrine processes, and fluvial networks provide evidence of recent or on-going fluvial processes (Barnes *et al.* 2007, Jaumann *et al.* 2008, Lorenz *et al.* 2008, Baugh 2008, Jaumann *et al.* 2009, Burr *et al.* 2009, Le Gall *et al.* 2010, Cartwright *et al.* 2011, Langhans *et al.* 2012).

External modification is in contrast to internal processes, for which the energy that drives the processes is supplied by internal heat of the planetary body. While evidence for on-going external processes is clear, evidence for internal modification of Titan's surface is ambiguous. Internal processes include volcanism and tectonism. Hypothesized cryovolcanic features such as Ganesa Macula, interpreted as a volcanic dome, and Winia Fluctus, interpreted as a volcanic flow (Sotin *et al.* 2005, Lopes *et al.* 2007, Wall *et al.* 2009) have been questioned or reinterpreted (Moore and Pappalardo 2011), although analysis of digital terrain models has strengthened the cryovolcanic hypothesis for some features, including Sotra Facula (Kirk et al. 2010, Lopes et al. 2011). Radar bright regions identified as eroded mountain chains (Radebaugh *et al.* 2007) represent no more than ~10% of Titan's surface based on recent mapping (Lopes *et al.* 2010), and the tectonic processes that formed these highlands are unclear. Although structurally controlled, Basin and Range-type mountains and valleys have been inferred in central Xanadu and attributed to regional extension (Radebaugh *et al.* 2011), no sources of tensional stress are specified. Lineaments interpreted as systems of conjugate faults have been identified in the Xanadu region (Paganelli *et al.* 2010), but the processes responsible for forming these lineaments are not discussed. Altimetry data showing steep breaks in topography close to the shoreline of Ontario Lacus suggest the presence of fault scarps, indicating that the lake may be contained within a graben or rift valley, but the processes responsible for producing graben in this area are not interpreted (Wall *et al.* 2010). In a preliminary investigation of structures as part of this work, features interpreted as folds and faults were found in Xanadu. Structural elements identified in the current data are thus putative, and the literature is lacking in discussion of tectonic processes and sources of stress. Possibilities include either that Titan does not have active, internally driven tectonic processes, or erosional and depositional processes erase tectonic features at the surface, or that Titan's crust may be new.

The work presented here was completed in collaboration with committee members Drs. Devon Burr, Josh Emery, and Bob Hatcher, UTK graduate student Richard Cartwright, MIT faculty Dr. Taylor Perron, MIT graduate student Ben Black, and Wheaton College faculty Dr. Geoff Collins. Dr. Burr supplied the idea for the project, research funding, and constructive feedback on this thesis, and contributed to mapping. Drs. Emery, Perron, and Collins provided constructive feedback on this thesis. Dr. Hatcher aided in interpretation of structural features and provided constructive feedback

on this thesis. Richard Cartwright contributed to mapping, performed drainage pattern classification for the Titan north polar networks, contributed to terrestrial network mapping and classification, and provided constructive feedback on this thesis. Ben Black contributed to mapping and provided constructive feedback on this thesis. I developed the methodology for data collection, drainage pattern classification, flow direction determination, and dominant azimuth orientation, performed the majority of the mapping and classification for Titan and terrestrial networks, determined flow direction and dominant azimuths, reviewed the literature for terrestrial analog network controls and performed all other tasks not listed here.

II. BACKGROUND: DATASETS AND DRAINAGE NETWORK TYPES AND CLASSIFICATION

2.1 Cassini-Huygens data of fluvial networks

Inferred fluvial features have been detected by three instruments onboard the Cassini spacecraft that image the surface of Titan: the Visual and Infrared Mapping Spectrometer (VIMS), operating at 300-5100 nanometers (Brown *et al.* 2004), the Imaging Subsystem for Science (ISS), operating over 200-1100 nanometers (Porco *et al.* 2005), and the Cassini Titan Radar Mapper (RADAR), emitting at 2.17 centimeters and collecting data in four modes, including synthetic aperture radar (SAR) images of the surface (Elachi *et al.* 2005). The datasets for these instruments have a range of spatial resolutions. VIMS and ISS have surface resolutions that vary with position and emission angle, but are commonly a few kilometers per pixel. SAR data are collected in swaths with the highest resolution in the center of the swath at closest approach and decreasing away from the center toward the ends of the swath. As a result, resolution ranges from ~350 meters per pixel at swath center to ~1.7 kilometers per pixel at the swath ends.

These SAR data are the highest resolution dataset available from Cassini. Although they cover only ~40% of the surface, compared to near-global coverage by the VIMS and ISS data, the SAR data provide the best resolution for mapping the fluvial networks and sufficient coverage to infer wide-spread distributions by network type. Radar swaths are referred to by their Titan flyby number; following this practice, I will refer to SAR data as T# throughout this thesis.

The fluvial networks observed in SAR data can be hundreds of kilometers long, tens to hundreds of kilometers wide, and display a variety of forms. Previous workers identified different types of networks. Initial network characterization with SAR data used albedo, width and length, and bright-dark pairing to describe the networks (Lorenz *et al.* 2008). Work by Burr *et al.* (2009) also used a simplified version of the quantitative Ichoku and Chorowicz algorithm and identified dendritic, parallel, and rectangular networks. Recent mapping of fluvial networks used a qualitative, visual classification scheme (Langhans *et al.* 2012).

Multiple fluvial networks were also observed by Huygens' Descent Imager/Spectral Radiometer (DISR, operating at 660 – 1000 nm) during the probe's descent to the surface of Titan (Tomasko *et al.* 2005, Soderblom *et al.* 2007a). Spatial resolution of the images improved as DISR approached the surface, ranging from 20-90 m/pixel during descent; on the surface, the resolution was several mm/ pixel (depending on distance). The networks detected by DISR (~5-15 kilometers in length, ~100 m in width for individual links) are significantly smaller than those detected by the RADAR instrument (SAR mode) and are not discernible in SAR data (Soderblom *et al.* 2007b)

Even within the limited area shown in the DISR mosaic of the Huygens landing site, the form of the fluvial networks varies. To the east, the drainage networks have longer and higher-order tributaries and more sinuous links. To the west, the drainage networks contain shorter, stubbier, lower-order tributaries (Tomasko *et al.* 2005, Soderblom *et al.* 2007a). This contrast in appearance was interpreted as resulting from differences in fluvial processes and controls (Soderblom *et al.* 2007a).

2.2 Drainage network types and classification

As on Titan, fluvial networks on Earth exhibit different morphologies that exist in a wide range of sizes. Network morphology, or drainage pattern, can provide information on regional slope, underlying structures, and bedrock characteristics through analysis of their patterns (Zernitz 1932, Thornbury 1954, Howard 1967, Morisawa 1985, Twidale 2004). Combinations of these geologic controls lead to the formation of identifiable drainage network patterns.

The significance of drainage patterns in determining regional geologic history has been known for over a century. Zernitz (1932) compiled previously published data on rivers around the world and qualitatively categorized them according to drainage pattern. She described six drainage patterns in detail, including in her analysis the form of the network in planview and the geologic controls on the pattern. She considered dendritic, trellis, rectangular, radial, annular, and parallel patterns the major drainage patterns. Dendritic drainage patterns form on rocks of homogeneous resistance and/or no consistent regional slopes; dendritic drainages tend to form in areas without structural controls, except in broad folds. Trellis drainage patterns form on tilted rocks of contrasting resistance. Rectangular drainage patterns form on rocks with approximately right angle fractures or faults, indicating a high degree of structural control. Radial drainage patterns form on uplifts as runoff moves downslope, away from the crest; the best examples of radial drainages form on the flanks of volcanoes as these features are very symmetric. Radial drainages are controlled primarily by slope. Annular drainage patterns form on rocks in mature domes, basins, or impact structures due to stream piracy of the original radial drainage; annular drainages imply structural control. Parallel drainage patterns form on rocks with a moderate to steep regional topographic slope or with parallel structures; thus parallel drainages can imply control by slope or structure. Zernitz included a discussion of “modified drainage patterns”: pinnate, subdendritic, anastomotic, and modified forms of trellis, rectangular, radial, and parallel patterns where multiple controls influence network form.

Thornbury (1954) also recognized the significance of drainage patterns, but his classification is different than that of Zernitz (1932). Thornbury (1954) considered the six major drainage patterns to be dendritic, trellis, barbed, rectangular, complex, and deranged. His definitions and geologic implications for dendritic, trellis, and rectangular patterns are identical to those of Zernitz (1932). He described barbed drainage patterns as being dominated by stream piracy, complex drainage patterns as those forming in areas of complicated structure and geologic history, and deranged drainage patterns as being poorly integrated streams that flow into/out of lakes or swamps. He considered a few of Zernitz’s major patterns to be “local patterns.” The four “local patterns” he recognized are centripetal, radial, parallel, and annular. His definitions and geologic implications for radial, parallel, and annular are identical to those of Zernitz (1932), although he pointed out that in the case of radial drainage, individual streams may have different patterns. Centripetal drainage patterns are described as those which converge in a central depression. This pattern is essentially the inverse of the radial pattern and is described also by Zernitz (1932) and Howard (1967) as a modified radial pattern.

In summarizing previous work on drainage network morphologies, Howard (1967) distinguished eight patterns as “basic drainage patterns:” dendritic, parallel, trellis, rectangular, radial, annular, multibasinal, and contorted. Of these eight patterns, the definitions and geologic implications of dendritic, parallel, trellis, rectangular, radial, and annular are the same as those of Zernitz (1932) and Thornbury (1954). The definitions of multibasinal and contorted given by Howard (1967) seem to conform to Thornbury's definitions and geologic contexts for deranged and complex, respectively. Like Zernitz (1932), Howard (1967) also recognized modified basic patterns where multiple controls influence network form.

Morisawa (1985) attributed drainage patterns to two geologic controls: structural and lithologic. She recognized nine basic drainage patterns: dendritic, pinnate, parallel, radial, trellis, rectangular, annular, centripetal, and distributary. Her definitions and geologic implications for dendritic, parallel, radial, trellis, rectangular, annular, and centripetal are identical to those of Zernitz (1932), Thornbury (1954), and Howard (1967). Zernitz (1932) and Howard (1967) considered the pinnate drainage pattern a modified dendritic pattern, being due to an easily eroded, homogeneous substrate. Howard (1967) also considered the distributary pattern a modified dendritic pattern. Howard (1967) and Morisawa (1985) defined the distributary pattern as forming where the trunk channel meets a low gradient area and streams diverge from the trunk.

Twidale (2004) identified nine patterns as basic drainage patterns: dendritic, parallel, radial, centrifugal, centripetal, distributary, angular, trellis, and annular. This group is similar to those described by Zernitz (1932), Thornbury (1954), Howard (1967), and Morisawa (1985), but Twidale introduced two new patterns: centrifugal and angular. Twidale's definitions and geologic implications for the other seven patterns are identical to those of previous authors. Twidale did not define the term "centrifugal," but other workers use it synonymously with "radial." The "angular" pattern is not quite identical to the “rectangular” pattern described by other workers; Twidale’s “angular” networks allow for links at sub-90° bends. This term is similar to the “angulate” pattern described by Zernitz (1932), Thornbury (1954), and Howard (1967). These authors considered the angulate pattern a modified version of the rectangular pattern where the controlling structures are not orthogonal. The geologic implications of the angulate pattern are intersecting fault or joint systems of different orientations or polygonal fracturing.

For this work, only three of the drainage patterns described above are focused on: dendritic, parallel, and rectangular. These drainage patterns are focused on because of the drainage patterns that can be detected using the quantitative drainage pattern classification algorithm described below, only these three are able to be detected on Titan due to the limitations of the current data resolution. The geologic implications for the basic drainage patterns able to be detected on Titan using the algorithm described below are summarized in Table 1.

Table 1. Basic drainage patterns.

Basic drainage patterns that can be detected with the modified drainage pattern classification algorithm, with geologic implications. The trellis pattern can be detected using the modified algorithm, but not with the data currently available.

Drainage Pattern	**Geologic Implications**
Dendritic	Uniformly resistant rocks and/or no consistent regional slope at time of drainage inception
Parallel	Moderate to steep regional slopes and/or parallel, elongate landforms
Trellis	Tilted layers of contrasting resistance to erosion
Rectangular	Joints and/or faults at near-right angles

2.3 Drainage pattern classification algorithm

From analysis of 198 pre-classified terrestrial networks, Ichoku and Chorowicz (1994) developed an empirical algorithm that identifies the network attributes and values that are diagnostic of five of the drainage pattern types recognized by the aforementioned workers (dendritic, parallel, trellis, rectangular, pinnate). Networks not meeting any of the specifications for these five patterns are considered “unclassified” by Ichoku and Chorowicz. Values of tributary junction angles, link lengths, link orientations, and proportion of right-angular bends, as well as “curvedness” and “meander” (defined below), are combined in a numerical algorithm to determine network patterns. These attributes can be measured in the field, from maps or from remotely sensed images of sufficiently high resolution.

At the low resolution of the SAR data, the character of the links comprising the drainage networks-whether river channels formed directly by flowing liquid, or river valleys that contain a smaller river channel within-cannot be determined (see Burr *et al.* 2012, in revision, for discussion). Such an inability to confidently discern river channels limits use of the algorithm of Ichoku and Chorowicz, because the full algorithm requires measure of channel “curvedness,” the ratio of the amplitude of a channel segment to its direct end-to-end distance, and “meander,” the ratio of the difference between the true length and arc length of a channel segment and its arc length (Ichoku and Chorowicz 1994). River channels may be more or less sinuous than the river valleys that host them (Leopold *et al.* 1964, Knighton 1998). This lack of certainty regarding the character of the links in Titan drainage networks, and resulting ignorance of channel curvedness and meander, means that the full algorithm cannot be used for Titan networks.

The Ichoku and Chorowicz algorithm can be simplified, however, to use only plan view characteristics that can be discerned and measured in remotely sensed images of Titan. This simplified algorithm (described in section 3.3) has been applied to a more limited dataset of Titan drainage networks (Burr *et al.* 2009). Patterns that can be detected using our modified algorithm are summarized in Figure 1. A flowchart of our simplified algorithm (Figure 2) shows both the diagnostic parameters that determine drainage network classification, and also the limitations on this technique of low-resolution data. For discussion of the limitations of this technique and our approach to potential misclassification, see section 5.2.

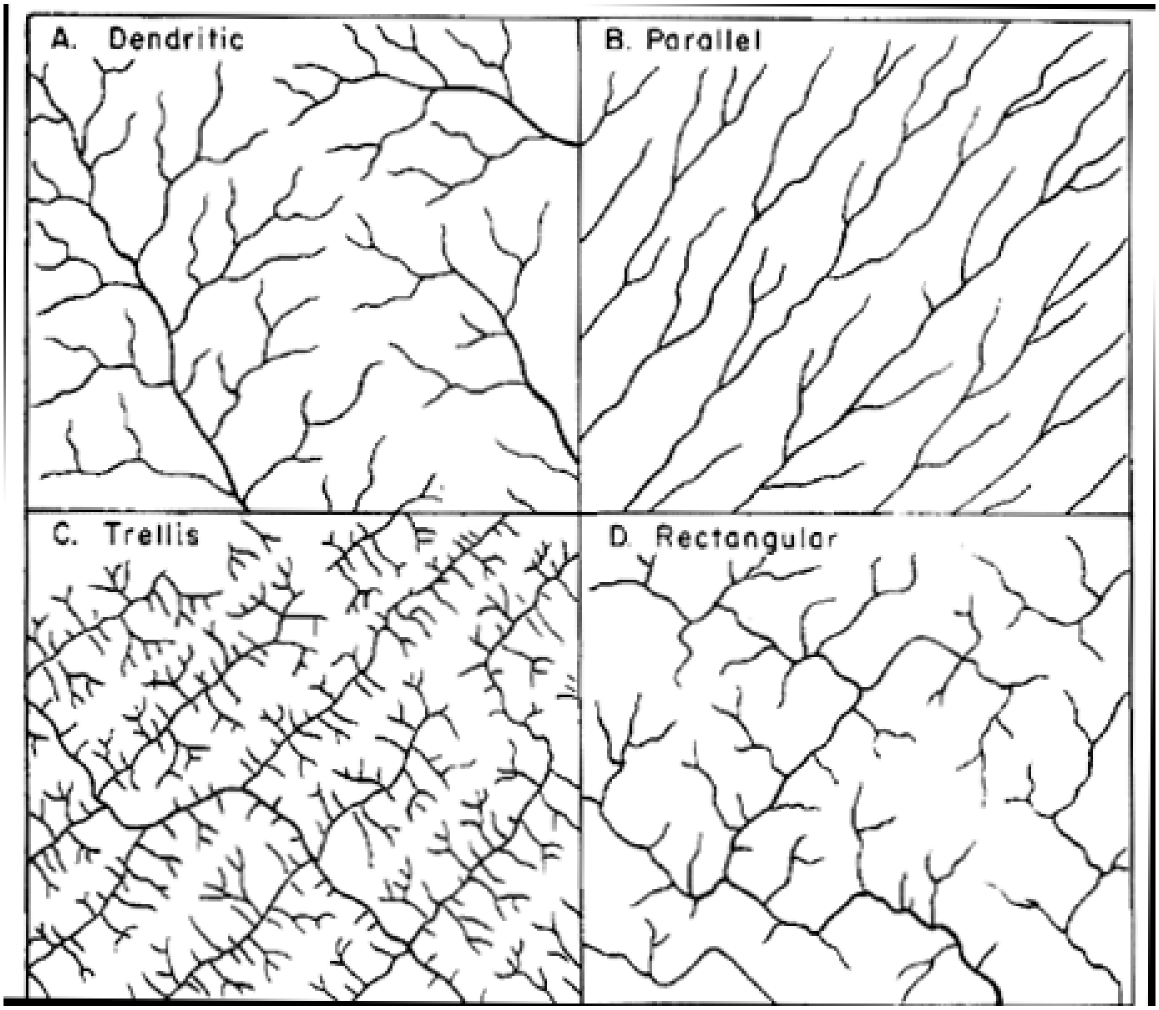

Figure 1. Basic drainage patterns discussed in this work.

Patterns that can be determined used our modified drainage pattern classification algorithm for Titan. With current data, trellis networks cannot be clearly identified, but with improved data, trellis network could be detected using the modified algorithm. Modified from Howard (1967).

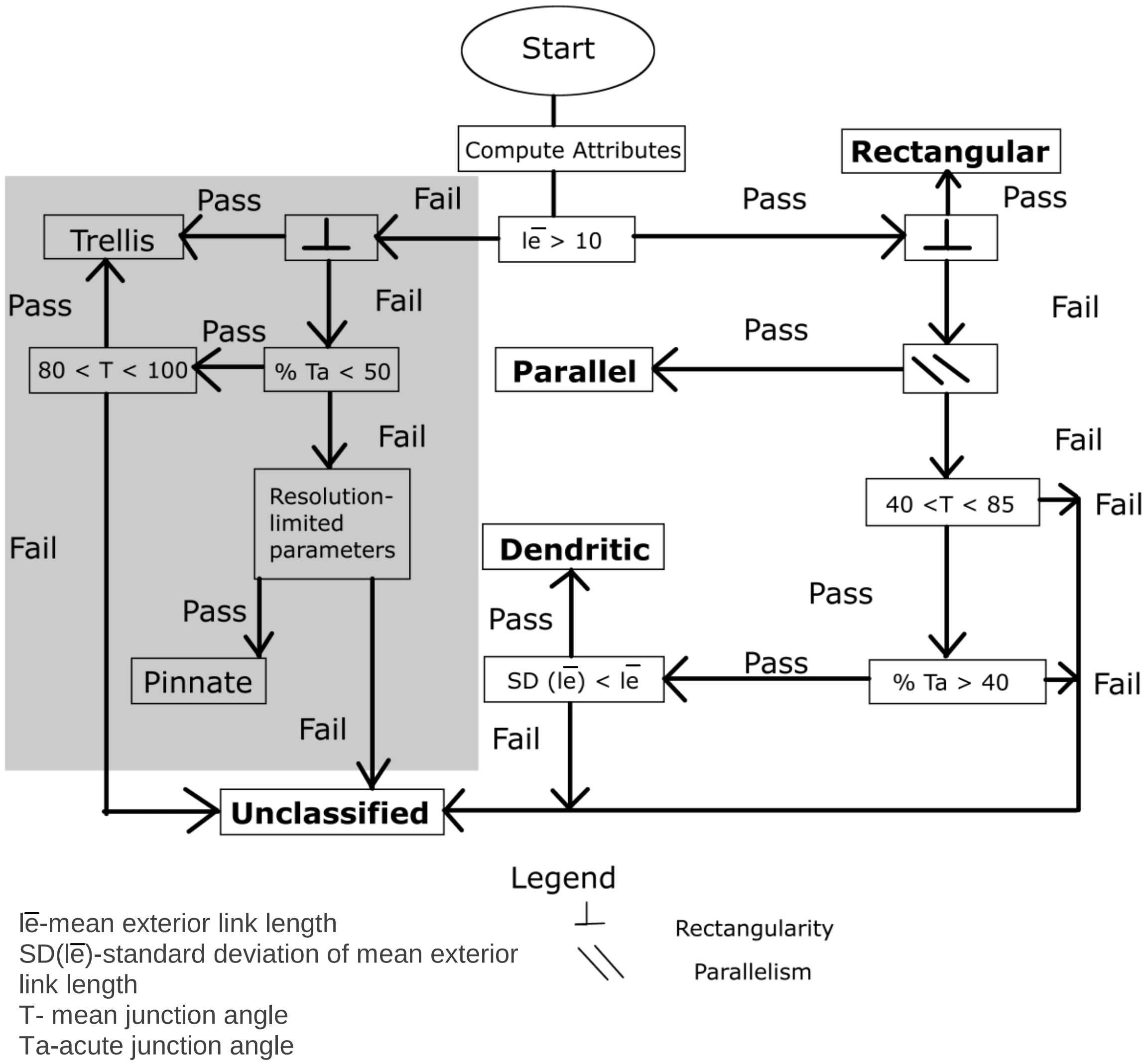

Figure 2. Modified algorithm for drainage pattern classification.

Updated algorithm for Titan, including trellis and pinnate classifications. "Resolution-limited parameters" includes channel curvedness and meander. The algorithm as used with current Titan is blind to the classifications on the left, covered by the gray box (see text for discussion).

2.4 Hypothesis and basic assumptions

I hypothesize that rectangular drainage networks on Titan are controlled by tectonic structures (joints and/or faults), specifically structures that have been formed by tensional stress. To test the hypothesis that the structures controlling Titan rectangular networks are extensional, networks on Earth qualitatively identified by other workers as rectangular, the structures controlling their morphology, and the origin of those structures were investigated. If the majority of terrestrial rectangular networks are controlled by structures that are extensional, the hypothesis will be considered supported. If the majority of controlling structures are compressional or strike-slip features, or there is no clear majority, the hypothesis will not be considered supported. This work is based on the following propositions: 1) that at Titan surface conditions ice has physical properties similar to rock (Collins *et al.* 2010 and references therein) and deforms in a brittle manner (Perron and de Pater 2004), so that stress regimes for structures on Titan can be inferred by comparison with terrestrial structures, and 2) that surficial flow and sediment transport on Titan is analogous to surficial flow and sediment transport on Earth (Burr *et al.* 2006) so that a terrestrial algorithm for fluvial network classification is valid for Titan networks.

Assumptions of a static crust, temporally unchanging stress field, and a single deformation event may be implicit in this work. Alternative scenarios to the hypothesis include fluvial control by compressional structures, strike-slip structures, or structures resulting from a combination of stresses (transtension, transpression). These alternative hypotheses could be tested by using high-resolution topographic data to make cross-sections over putative structures, high-resolution SAR data to identify displaced features, or increased SAR coverage to identify macro-scale displacements. Titan's crust and stress field orientation have likely changed through time as a result of change in orbital dynamics. There have most likely been multiple deformation events that created structures on Titan. These possibilities could be tested by comparing orientations of link segments of rectangular fluvial networks to test for a uniform stress field, and looking for cross-cutting structures to test for multiple deformation events. Areas of young, featureless crust may be indicative of crustal regeneration. Increased resolution of SAR data and increased SAR coverage would help in testing these alternatives.

III. METHODS AND DATA

3.1 Mapping

Drainage networks on Titan captured in both SAR and DISR data were analyzed. For the SAR data analysis, all SAR swaths through the T71 fly-by on July 7, 2010, were mapped prior to a year-long hiatus in SAR data collection, to delineate fluvial networks. This mapping was done using ESRI's ArcMap software. Individual features were mapped based on a set of three criteria derived from previous work (Barnes *et al.* 2007, Lorenz *et al.* 2008, Burr *et al.* 2009): (a) distinguishability in tone from the surrounding terrain, (b) a bright/dark pairing indicative of a depression, and (c) fluviatile morphology (defined as sinuous and/or branching). Features meeting two or more of the criteria were mapped as "known;" features meeting one criterion were mapped as "uncertain;" and where features were discontinuous over distances less than ~10 km, the discontinuous sections were mapped as "inferred" (Figure 3), and some networks contain more than one level of certainty. Networks consisting of a majority "uncertain" and "inferred" links were not included in drainage pattern analysis.

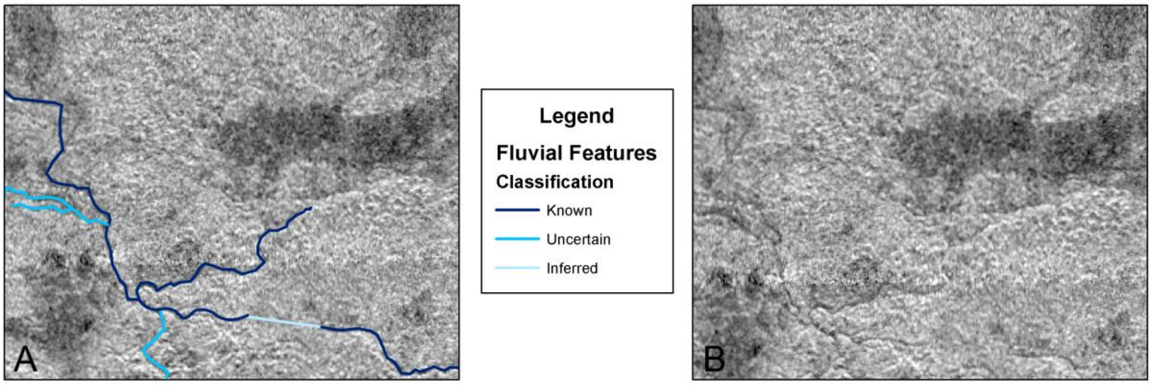

Figure 3. Example of mapping categories.

A portion of a network with examples of each mapping category: known, uncertain, inferred (A). (B) The same network without mapping overlain. Center of figure is approximately 87°W, 10°S in T13 radar swath.

The effect of different radar illumination azimuths on network classifications was explored by comparing classification results where possible for overlapping swaths. There are 40 areas of swath overlap, but most areas of overlap either do not contain networks or contain networks below the size threshold for classification (see section 3.3 for discussion of size threshold). In some areas, overlapping swaths have large differences in resolution. For example, swaths T25, T28, and T29 have nearly identical radar illumination azimuths, but show significant differences in feature delineation on the T25 swath compared to the T28/T29 swaths. These differences in mapping are attributed to the very poor resolution of the T25 swath compared to the T28 and T29 swaths, which have high, nearly identical resolutions. Overall, however, differences in radar illumination azimuth result in only slight differences in feature delineation in overlapping swaths. The T64 radar swath also has areas of overlap with the T25, T28, and T29 radar swaths, but those areas of overlap are not amenable to network classification due to areas of missing data in the area of overlap. One possible test case in southwestern Xanadu is covered by both T13 and T44 at similar resolutions, with illumination azimuths that differ by ~45 degrees, and shows large enough networks to be classified. The findings verify previous work (Burr *et al.* 2009) that although the network mapping differed slightly between swaths, the classifications of the networks from the two different swaths were the same; however, this is the only example of a test for different radar illumination azimuths.

After mapping was complete, separate equidistant projections (for measuring length) and equal angle projections (for measuring angles) were made for each swath as appropriate for the swath latitude (Table 2), and the length and orientation data for use in the modified classification algorithm (Figure 2) were collected using Jennessent Graphic Tools and Shapes plug-in for ArcMap. For 60°N-60°S, cylindrical equidistant projections were used for measuring length and Mercator projections were used for measuring angles. For the north and south poles, polar stereographic projections were used for measuring both length and angles.

For analysis of the drainage networks observed in the DISR data, the DISR mosaic from an altitude of eight kilometers from Tomasko *et al.* (2005) was used and cropped to include only the area with networks. The fluvial features in the mosaic were mapped in ArcMap using two of the three criteria described above-namely, distinguishability in tone and fluviatile morphology-but because these data were taken under the diffuse lighting conditions at Titan's surface, and using a passive sensor as opposed to an active sensor, the third criterion (bright/dark pairing indicative of shadowing) does not apply. Features meeting two of the two remaining criteria were mapped as known, and features meeting one of these criteria were mapped as uncertain. Because the mosaic does not contain geographic reference information, the ArcMap measurements may have small errors. However, because the area covered is so small, any error introduced is considered minimal, consistent with previous use of this mosaic (Tomasko *et al.* 2005, Perron *et al.* 2006, Soderblom *et al.* 2007a).

Table 2. Projections for measurements.

Proper projections for parameters measured for the appropriate latitude ranges.

Latitude range	**Projection**	**Parameter measured**
60°-90° N, 60°-90° S	Stereographic north/south polar	Length, angle
60°N - 60°S	Equidistant cylindrical	Length
60°N - 60°S	Mercator	Angle

3.2 Flow direction

Direction of flow provides information on the direction of the slope. This indirect evidence is useful for understanding Titan's topography as elevation data are sparse. Flow direction was determined using networks that met one of three criteria: a) acute junction angles pointing in a consistent direction, b) adjacent lakes (Stofan *et al.* 2007, Hayes *et al.* 2010), and c) adjacent hypothesized sedimentary deposits (Jaumann *et al.* 2008, Lorenz *et al.* 2008).

3.3 Drainage pattern analysis

Drainage pattern analysis for both SAR and DISR networks was done using the modified algorithm (Figure 2). The necessary input parameters for the algorithm are a combination of network attributes including lengths and azimuths of network links, junction angles of first order tributaries, percent of right angle (80°-100°) bends, and percent of acute (< 80°) junction angles in the network. After attributes are computed, if the mean exterior link length is longer than 10 pixels, the network passes to the right side of the algorithm in Figure 2 and is tested for rectangularity, parallelism, and dendritic morphology. There are three separate tests for rectangularity: 1) ≥ 20% of links have right angular bends, 2) ≥ 50% of Strahler order 2 links have right angular bends, 3) for 30° bins of the data, any two orthogonal bins have the two highest link length totals. Because it is not known if the Strahler order 2 links are truly second order, for test (2) any interior link was considered. If a network passes *any one* of these three tests, it is classified as rectangular. If not, it continues to the parallelism test.

There are likewise three separate tests for parallelism: 1) ≥ 60% of total exterior link length fall within a single 30° bin, 2) the sum of any two adjacent 30° bins is ≥ 70% of total exterior link length, 3) the total exterior link length in any two adjacent 30° bins is ≥ 50% and the total interior link length in the same two bins is ≥ 80%. If the network passes *any one* of these three tests, it is classified as parallel. If not, it continues to the tests for a dendritic network.

There are three combined tests to determine whether a network is dendritic: 1) the mean junction angle is between 40° and 85°, 2) ≥ 40% of junction angles are acute, 3) the standard deviation of mean exterior link length is less than the mean exterior link length. If it passes *all three* dendritic tests, it is classified as dendritic. If it fails any of these tests, the network remains unclassified.

If the mean exterior link length is less than 10 pixels, the network goes to the left side of the algorithm which includes trellis and pinnate. These networks types cannot be detected with this algorithm due to the resolution limits of the SAR data. See Ichoku and Chorowicz (1994) for more information about the original algorithm, as well as discussion of the limits of the modified algorithm in section 5.2.

The algorithm may produce invalid results due to a low number of data points for a given network, although a quantitative cutoff is not provided in the original work (Ichoku and Chorowicz 1994). Mejía and Niemann (2008) suggest that only networks of sixth and higher Strahler orders are amenable to analysis using the algorithm designed by Ichoku and Chorowicz (1994), although the justification for this threshold is not described. Strahler stream ordering is a network ordering system wherein all fingertip tributaries are assigned order “1” and where links of equivalent order (n) join, the order of the downstream link is (n+1). In comparison, Shreve magnitude is a network ordering system wherein each fingertip tributary is assigned an order of 1, and the order of the downstream link is simply the sum of the orders of the contributing upstream links.

To assess whether the analysis used is valid for the smallest networks in this study, the distribution of network types was compared for the smallest networks to that for the largest networks. An arbitrary minimum of 10 links per network was chosen, for which the lowest possible Shreve magnitude is 6. Given that Strahler stream orders are always equal to or commonly much larger than Shreve magnitudes for the same network, a minimum Shreve magnitude of 6 ensures that the suggestion of Mejía and Niemann (2008) is met. Shreve magnitudes were determined only for networks for which flow direction could be determined. Thus, Shreve magnitudes could be determined for 45 of the 48 SAR networks.

These 45 networks were divided into three groups that contain approximately equal numbers of networks: Shreve magnitudes 6-7, 8-13, and 14-51. Against the group of the largest Shreve magnitudes, for which the classification percentages are considered to be reliable, the classification percentages for the group with the smallest Shreve magnitudes were compared. For the four classifications (rectangular, dendritic, parallel, and unclassified), the root mean square (RMS) for the difference between those two groups was computed as

$$RMS = \sqrt{((x_1 - y_1)^2 + (x_2 - y_2)^2 + (x_3 - y_3)^2 + (x_4 - y_4)^2)/4}$$

where 1, 2, 3, and 4, represent the four classifications. The RMS value for the dataset is 5%.

Next, a Monte Carlo simulation was used to compute the classification percentages for four classifications sampled at random and the distribution of RMS differences was calculated from classifications for the Shreve magnitude 14-51 networks. I then compared the actual RMS value for the smallest networks (5%) against the probability distribution of RMS values from random sampling. The likelihood of an RMS value equal to 5% is approximately 0.002 or 0.2%, or greater than three standard deviations away from the modal value. Based on this calculation, it is concluded that the minimum threshold of 10 links, equal to a minimum Shreve magnitude of 6, is representative of the networks with the highest Shreve magnitudes (14-51). Total percentages reported throughout this work are the classification percentages of all 48 SAR networks with 10 or more links that were classified. This numerical algorithm for network classification is used in order to provide quantitative definitions and parameters for each drainage pattern and to follow a consistent, unbiased classification for ourselves and future workers. As the quality of the Titan SAR data is variable and often poor, using a numerical algorithm aids in determining drainage patterns that may be difficult to distinguish visually in the SAR data. Also, use of SAR data for geomorphic analyses is much less common for the Earth and Mars, due to the availability of high resolution aerial imagery, so use of a numerical algorithm for drainage pattern classification would be useful for comparative planetology.

3.4 Network statistics

During mapping, networks were ordered using the Shreve magnitude system. Total lengths for each network were computed by adding the lengths of all networks links acquired using the Jennessent Graphic Tools and Shapes plug-in. For each network classification that is able to be detected: dendritic, parallel, rectangular, and unclassified networks.the Shreve magnitudes and total network lengths were averaged and used as a proxy for network size and degree of incision to make a general comparison among the four patterns.

3.5 Terrestrial drainage pattern analysis

To explore the tectonic stresses associated with the rectangular networks on Titan, rectangular networks on Earth were analyzed. First, terrestrial networks qualitatively classified in the network classification literature cited in section 2.2 to be rectangular were selected and their classification was verified with the algorithm. Then the stresses that cause their controlling structures were determined from the literature. The reach of the Zambezi River between Victoria Falls and Lake Malawi (Zernitz 1932, Twidale 2004), the Yellowstone River between Yellowstone Lake and the Grand Canyon of the Yellowstone (Zernitz 1932), the Schroon River reach southwest of Elizabethtown, NY (Zernitz 1932, Thornbury 1954, Howard 1967, Morisawa 1985), and the Katherine River north of Katherine, Northern Territory, Australia (Twidale 2004) were used in this investigation. The Murchison River near Carnarvon, Western Australia (Twidale 2004), was mapped for use in this investigation and confirmed to be rectangular, but lack of sufficient data on the origin of the controlling joints led to the exclusion of this river from the terrestrial dataset. This selection includes rivers on three continents and in four different climates providing a range of conditions. The networks were mapped in ArcMap on aerial photos and topography, including 15-meter resolution Landsat 7 images and 10-meter resolution National Elevation Dataset data. Necessary networks attributes were obtained in ArcMap using the Jennessent Graphic Tools and Shapes plug-in.

IV. RESULTS

4.1 Flow direction

Results of flow direction analysis (Figure 4) indicate both broad trends in flow direction as well as local effects. Flow is generally southerly in the Xanadu region, with deflection to the east and west along the perimeter, according to the location of Xanadu given in Radebaugh *et al.* (2011). Networks adjacent to Ontario Lacus in T56 appear to flow south into the lake. Other than at Ontario Lacus, in the south polar region, there is not a clear trend in flow direction. In the north polar region, all networks appear to flow into the large lakes. Flow in the northern hemisphere is broadly northeastwards, with the exception of small networks on the east rim of Menrva crater. Flow direction, where determination was possible, is marked by black arrows in Figure 4. Areas with possible distributary networks or ambiguous flow direction were marked with double-headed arrows, where flow is assumed in the orientation of the long dimension of the network but the direction of flow is uncertain.

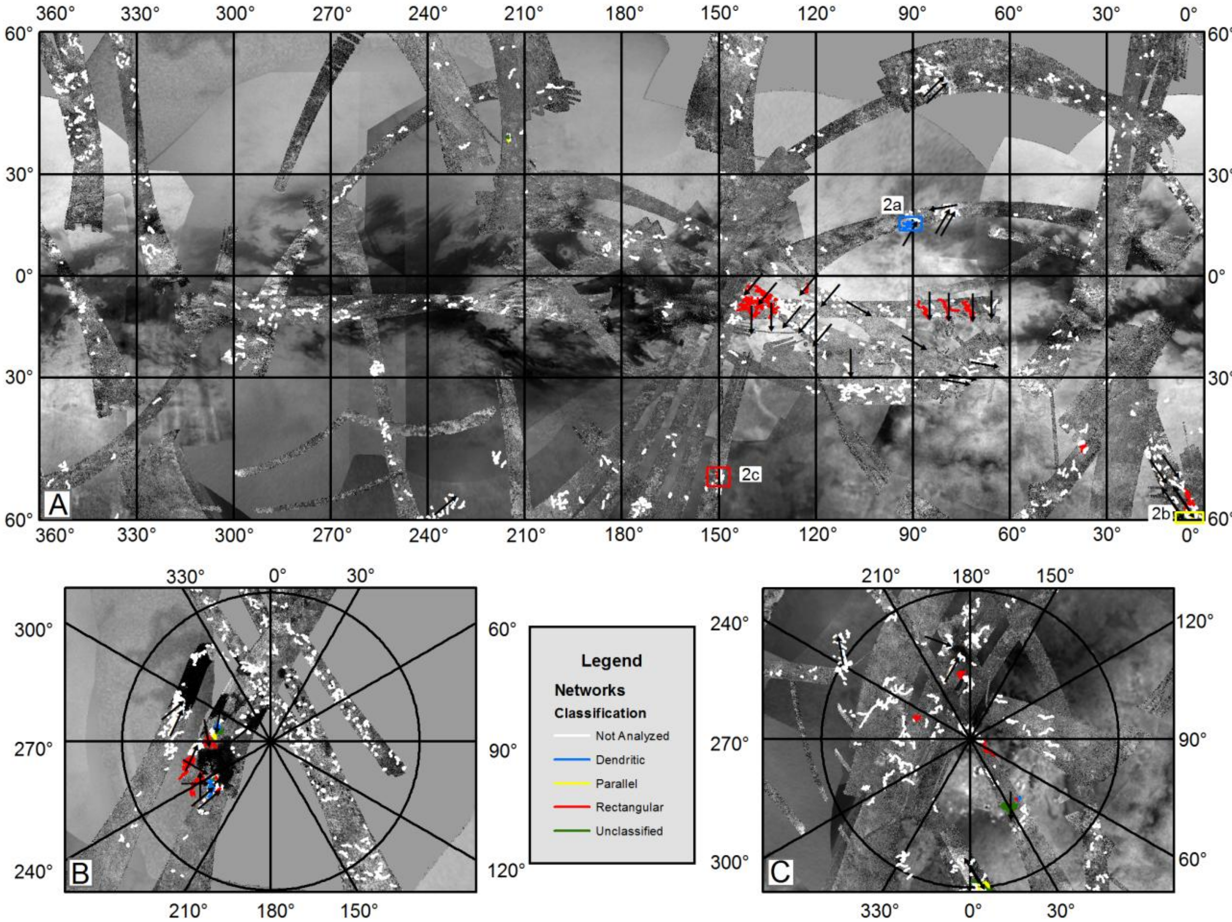

Figure 4. Geographic distribution of networks classified in this work.

As classified in this work, blue networks are dendritic, yellow networks are parallel, red networks are rectangular, and green networks are unclassified. White networks are those that fall below the size criteria for classification and therefore were not classified. Black arrows indicate flow direction for networks that meet at least one criterion for determining flow direction. Where direction is not clear, double-headed arrows are used (60°S, 5°W). (A) Networks between 60°N and 60°S. (B) Networks in the north polar region between 60°N and 90°N. (C) Networks in the south polar region between 60°S and 90°S. 10° of longitude is equal to 450 kilometers.

4.2 Drainage pattern classification

After all the fluvial features observed in the radar swaths and DISR mosaic were mapped, the modified algorithm was applied only to networks with a minimum of 10 links, where the total is 53 (48 SAR networks and five DISR networks) (Table 3). Of the 48 SAR networks, twelve networks (25%) were classified as dendritic, implying the presence of a gentle regional slope at the time of drainage inception and/or homogeneous nonfractured bedrock. Four networks (8%) were classified as parallel, implying moderate to steep slopes or the presence of parallel, elongate landforms. Twenty-seven networks (56%) were classified as rectangular, implying the presence of joints or faults at approximately right angles. Classified networks exhibit a wide range of stream order and drainage basin size. Classifications of networks in areas previously analyzed by Burr *et al.* (2009) were consistent with the exception of one network in the T41 radar swath, which was not analyzed because it contained fewer than 10 links. Five networks (10%) fell into the “unclassified” category (Table 3).

Table 3. Percentages of drainage patterns.

SAR and DISR networks with number of networks and percent of total networks.

SAR Networks		
Pattern	**Total Networks**	**Percent**
Dendritic	12	25%
Parallel	4	8%
Rectangular	27	56%
Unclassified	5	10%
DISR Networks		
Pattern	**Total Networks**	**Percent**
Dendritic	0	0%
Parallel	0	0%
Rectangular	5	100%
Unclassified	0	0%

"Unclassified" networks have no specific geologic implication; in fact, there are several reasons a network may be "unclassified." Anomalous networks, large networks with sub-basins of different network morphologies, or network patterns not characterized by Ichoku and Chorowicz may all result in being "unclassified" according to our modified algorithm. Of the five networks analyzed at the Huygens landing site (Figure 5), all five (100%) were classified as rectangular (Table 4). While the only drainage patterns found in our study were dendritic, parallel, and rectangular, annular networks have been qualitatively identified along the shoreline of Ligeia Mare (Wasiak *et al.* 2012). The algorithm yielded rectangular classifications for these networks; however, the algorithm does not include tests for the annular pattern, so that pattern cannot be detected.

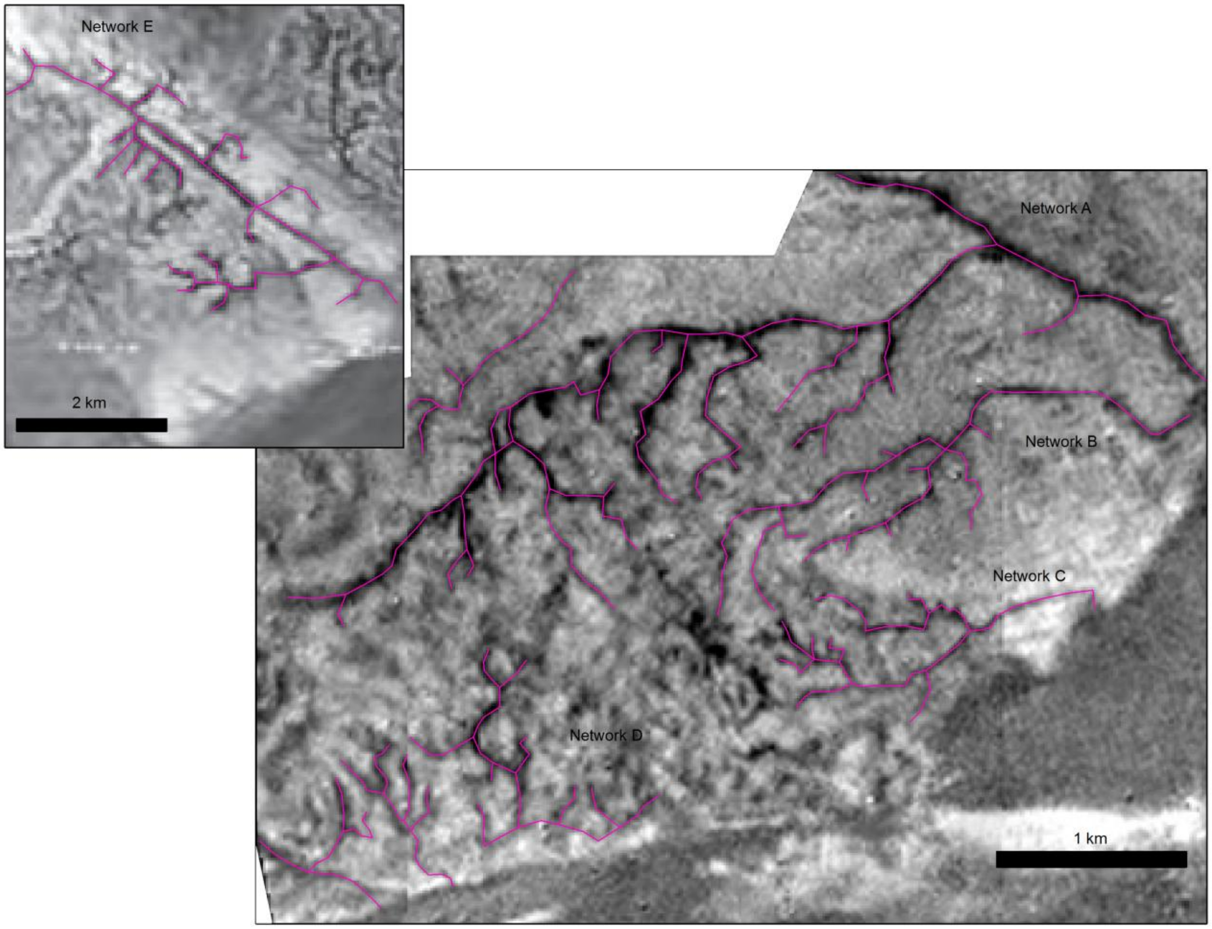

Figure 5. Huygens Landing Site networks.

Mapping of five networks along Huygens Landing Site "coastline" at (10°S, 192°W,).

Network in upper left box is located west of four networks in lower right box.

Table 4. Summary of classified networks.

Lat/long pairs are approximate centers of networks to the nearest degree. Shreve magnitudes are minimum values as true first order tributaries cannot be detected in SAR data. The networks without data for Shreve magnitudes are those for which flow direction is uncertain. The Huygens Landing Site networks do not have total lengths because geographic reference information is not available for the mosaic used.

Network	Long.	Lat.	Classification	Observed Shreve Magnitude	Total length of network links (km)
T3 A	90°W	15°N	Dendritic	17	808
T28 C(2)	237°W	75°N	Dendritic	8	60
T29 D	236°W	75°N	Dendritic	12	99
T29 F	233°W	74°N	Dendritic	7	83
T29 H	231°W	74°N	Dendritic	44	412
T28 L	283°W	79°N	Dendritic	34	410
T28 R	276°W	76°N	Dendritic	11	171
T28 V	259°W	75°N	Dendritic	7	40
T39 F	40°W	74°S	Dendritic	9	103
T64 A	236°W	75°N	Dendritic	6	60
T29 E	234°W	75°N	Dendritic	6	40
T28 M	280°W	80°N	Dendritic	21	194
T7 C	4°W	59°S	Parallel		165
T28 N	275°W	78°N	Parallel	10	151
T28 T	248°W	76°N	Parallel	7	79
T64 C	215°W	39°N	Parallel	6	66
T7 D	7°W	55°S	Rectangular		459
T13 A	73°W	10°S	Rectangular	16	919
T13 B	134°W	10°S	Rectangular	18	1255
T13 C	140°W	10°S	Rectangular	43	2631
T13 D	86°W	11°S	Rectangular	8	394
T13 E	80°W	10°S	Rectangular	6	307
T28 A	242°W	72°N	Rectangular	22	690
T29 B	236°W	77°N	Rectangular	14	65
T29 G	227°W	75°N	Rectangular	18	211

Table 3 (cont.) Summary of classified networks.

Network	Long.	Lat.	Classification	Observed Shreve Magnitude	Total length of network link (km)
T28 I	265°W	79°N	Rectangular	9	114
T28 J	266°W	78°N	Rectangular	6	111
T28 O	269°W	77°N	Rectangular	17	292
T28 P	256°W	73°N	Rectangular	51	1042
T28 S	246°W	76°N	Rectangular	13	113
T28 U	276°W	77°N	Rectangular	9	201
T36 A	37°W	47°S	Rectangular	10	376
T39 A	211°W	54°S	Rectangular	7	174
T39 D	57°W	86°S	Rectangular	6	325
T39 H	37°W	74°S	Rectangular	6	38
T43 A	124°W	4°S	Rectangular	5	375
T44 B	141°W	4°S	Rectangular	9	366
T44 C	136°W	6°S	Rectangular	26	843
T44 D	135°W	8°S	Rectangular	12	953
T58 B	188°W	77°S	Rectangular	7	307
T58 C	248°W	78°	Rectangular	9	253
T59 A	150°W	53°S	Rectangular	7	126
T59 B	150°W	52°S	Rectangular	10	82
T7 B	5°W	60°S	Unclassified		457
T29 C(1)	237°W	76°N	Unclassified	10	78
T28 Q	276°W	76°N	Unclassified	38	337
T39 G	29°W	73°S	Unclassified	36	908
T64 B	215°W	40°N	Unclassified	12	105
HLS A	193°W	10°S	Rectangular	19	
HLS B	193°W	10°S	Rectangular	11	
HLS C	193°W	10°S	Rectangular	8	
HLS D	193°W	10°S	Rectangular	8	
HLS E	193°W	10°S	Rectangular	17	

Although not analyzed, networks with fewer than ten links are not insignificant, as small networks and individual features account for approximately 82,000 kilometers of length in total, compared to the analyzed networks which only account for 18,275 kilometers of length in total. Combined length of analyzed and unanalyzed networks is approximately 100,000 kilometers. This combined length is more than four times the combined length reported in previous mapping efforts with a less complete dataset (Langhans *et al.* 2012). Improved denoising of RADAR images (e.g., using the techniques of Lucas *et al.* 2011, Lucas *et al.* 2012) may reveal sufficient detail to provide more comprehensive mapping of networks, as was accomplished with higher resolution data for valley networks on Mars (e.g., Hynek and Phillips 2003). This technique may resolve lower-order tributaries. If so, networks with fewer than 10 links in the current data, and therefore not included in this classification, may be large enough to include in future classifications. Also, inclusion of short, lower-order tributaries may make it possible to use the left side of the modified algorithm (Figure 2) that is currently inaccessible.

4.3 Geographic distribution of networks by type

In available SAR coverage, networks are widespread, but drainage pattern types are not equally distributed (Figure 4). Both dendritic and parallel networks are predominantly polar. Of the dendritic networks, eleven (of twelve) are located poleward of 60° (Figure 6). Of the parallel networks, three (of four) are in polar regions. Four (of five) of the unclassified networks are at or poleward of 60°. In contrast, the networks classified as rectangular are more global in distribution: one-third (8043 km) are located in Xanadu, between 10°N and 10°S, one-third are located above 60°N (2839 km), and one-third are located in the southern mid-latitudes and south polar region (2140 km).

A parameter, "mapped fluvial feature density," is defined as the total distance along mapped fluvial network links in bands of 30° latitude divided by the area of SAR coverage in those latitude bands. This parameter has units of m/km^2 and differs from drainage density in two ways: 1) our mapped distance may represent river valleys instead of river channel lengths, and 2) given the lack of topographic information or data resolution needed to define drainage basin area, the parameter normalizes total length by total geographic area coverage instead of by drainage basin area. Lengths and areas were calculated using ArcMap. The mapped fluvial feature density gives a quantitative parameter by which to assess the pervasiveness of fluvial modification discernible at the resolution of the SAR data. The polar regions have the highest mapped fluvial feature density. The southern mid-latitudes (60°S - 30°S) and tropics (30°S - 0°S) have the next highest density. The northern mid-latitudes (30°N - 60°N) and the tropics (0°N - 30°N) have the lowest mapped feature density (Table 5). The difference between the highest and lowest values is one order of magnitude.

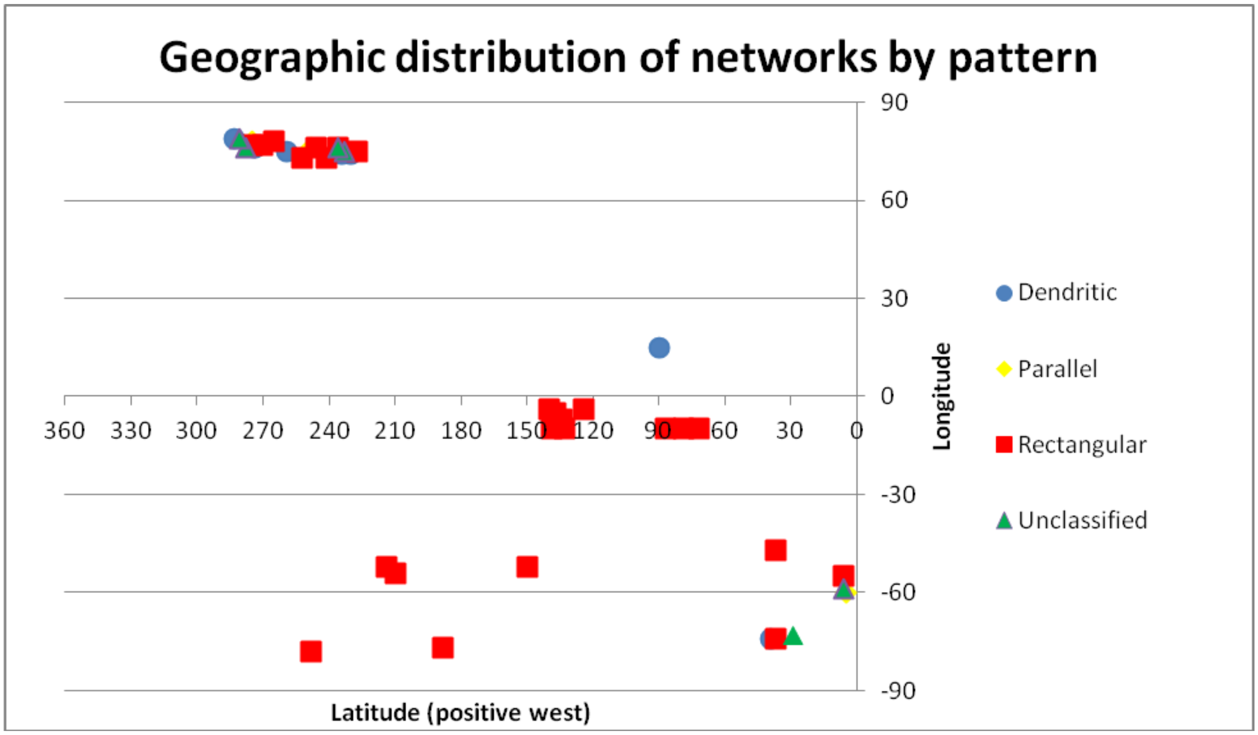

Figure 6. Geographic distribution of networks by pattern.

Points represent centers of networks.

A nearest neighbor analysis was used to determine randomness of the geographic distribution of the analyzed networks by measuring the distance from the center of a network to the next closest network in ArcMap (Figure 6). At a significance level of 5%, the analyzed networks do not have a random distribution, and are clustered at the poles and equator. This analysis does not take into account the possible effects of uneven SAR coverage.

Table 5. Mapped fluvial feature density.

Mapped fluvial feature density organized by latitudinal bands of 30°.

Latitude	Mapped fluvial feature density (m/km²)
60°-90° N	19
30°-60° N	2.5
0°-30° N	1.1
30°-0° S	3.1
60°-30° S	3.2
90°-60° S	7.1

4.4 Network link orientation

Rose diagrams showing network link orientations as a function of link length were produced for each network analyzed. Petal length is a function of the cumulative length of links (interior and exterior) within a given 5° azimuth bin. Generally, rose diagrams for dendritic networks lack preferred orientations, instead showing that links have many orientations spread around a central azimuth oriented along the long dimension of the network (Figure 7A). Rose diagrams for parallel networks show a strong preference for one orientation spanning ~30° around the network azimuth (Figure 7B). Rectangular networks show many orientations with typically two to four preferred orientations (Figure 7C).

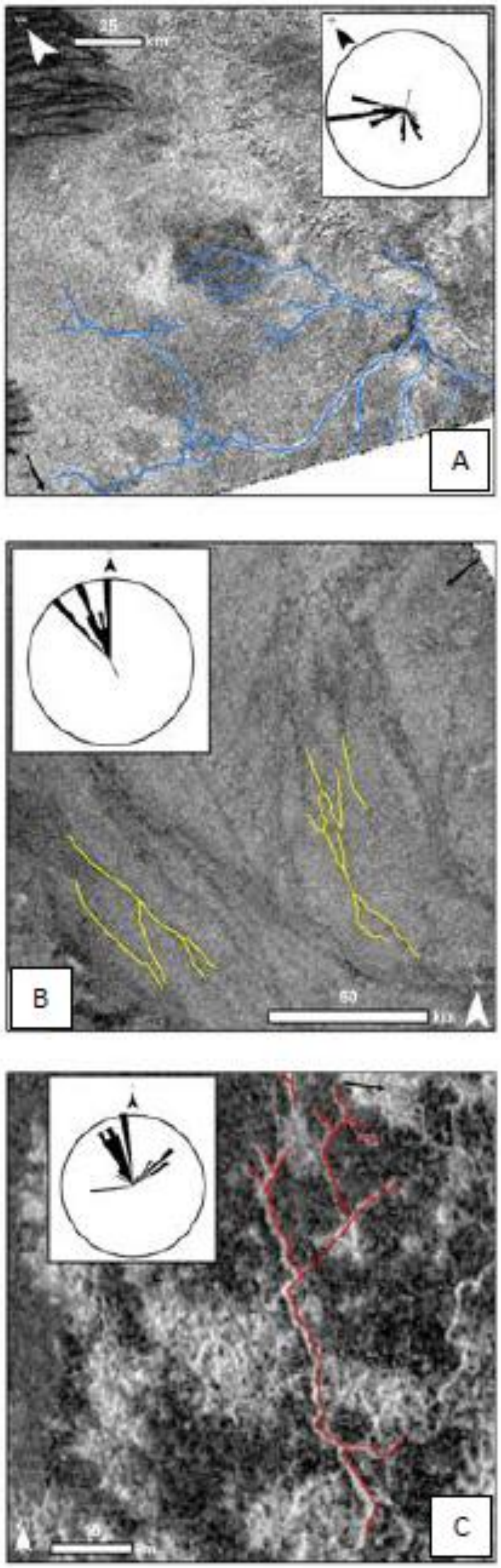
A
B
C

Figure 7. Examples of drainage patterns and link orientations. (A) Dendritic network in the T3 swath with rose diagram. Image centered on 15°N, 90°W, (B) Two parallel networks in T7 swath with rose diagram. The rose diagram includes both yellow networks. Image centered on 59°S, 4°W, (C) Rectangular network in the T59 swath with rose diagram. Image centered at 52°S, 150°W. Black arrows indicate direction of radar illumination.

Preferred orientations vary by latitude (Table 6). In the southern hemisphere, these orientations are largely uniform by latitude: in the southern polar region, dominant link orientations in rectangular networks fall within 15 degrees of each other, and within 10 degrees of each other in the mid-latitudes. More variation is apparent in the southern tropics-coincident with southern Xanadu-, where the orientations fall along two directions, NW-SE (136°-150°) and NNE-SSW (11°-20°). No rectangular networks were mapped in the northern tropics or mid-latitudes. The rectangular networks in the north polar region show the greatest variation in orientation, presumably because of the local influence on drainage of the lakes. These trends are consistent with previous analysis of more limited rectangular network link orientations by Burr *et al.* (2009), as well as more localized analysis of structural elements in the Xanadu region by Paganelli *et al.* (2010). Liu *et al.* (2012) measured orientations of equatorial mountain chains at 30°W, Xanadu, 200°W, and 300°W. At 30°W, 200°W, and 300°W, mountain chains have consistent east-west orientations of 80° and 102°. However, mountains in Xanadu have more variation in orientation, which is consistent with the variation seen in rectangular network link orientation in Xanadu.

Table 6. Dominant link orientations for rectangular networks.

Dominant orientations of links in rectangular networks organized by latitude band. Arrows indicate direction of link orientations. Orientations listed in order of strength of preference.

Latitude	**Dominant Azimuths**
60°N-90°N	101°-105°, 156°-160°, 146°-150°, 71°-75°, 151°-155°, 76°-80°, 111°-115°
30°N-60°N	No rectangular networks
0°N-30°N	No rectangular networks
0°S-30°S	146°-150°, 11°-15°, 141°-145°, 16°-20°, 136°-140°
30°S-60°S	161°-165°, 151°-155°
60°S-90°S	56°-60°, 66°-70°, 61°-65°

4.5 Network statistics

Dendritic networks are well-integrated with a mean Shreve magnitude of 16 and a mean network summed length of 225 kilometers. Parallel networks are the least-integrated of the classifications with a mean Shreve magnitude of 9 and a mean network summed length of 132 kilometers. Rectangular networks are comparable to dendritic networks with a mean Shreve magnitude of 14, but have a larger mean summed length of 482 kilometers. Unclassified networks have the highest mean Shreve magnitude of 22 and the second highest summed network length of 336 kilometers (Figure 8).

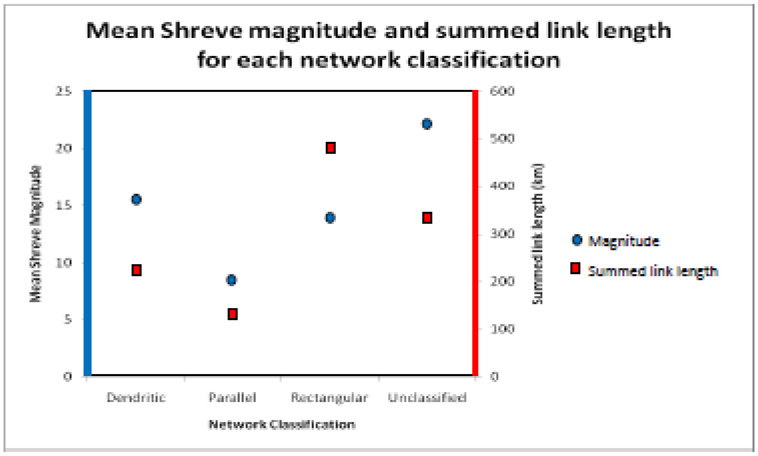

Figure 8. Network statistics.

Mean Shreve magnitudes and mean summed network link lengths on Titan for each network classification type.

4.6 Terrestrial analog study

The four terrestrial rivers included in this investigation, the Yellowstone River, Schroon River, Zambezi River, and Katherine River, were all confirmed as rectangular networks using the modified algorithm developed for Titan (Figure 9). A review of the literature on the controlling structures and the origin of those structures for each river revealed that all four rivers are controlled by extensional structures. Summaries of the regional geology, network controls, and sources of stress are given below for each river.

Yellowstone River: The Yellowstone River flows through Yellowstone National Park in northwestern Wyoming, U.S.A. The national park boundary is located around the Yellowstone Caldera, which includes two resurgent domes: the Sour Creek and Mallard Lake Domes. This volcanic province is a relatively young feature in the area with three eruptions in the last two million years (Christiansen 2001).

The river features sharp right-angle bends and straight links trending NE-SW and NW-SE. According to Christiansen (2001; p. G110), the areas of the river that feature these right-angle bends are controlled by graben. These graben are a result of uplift due to magmatic recharge of the Sour Creek Dome, creating tensional stress in the overlying rock, to the point of creating faults and causing earthquakes (Chang *et al.* 2007). The primary axis of the dome follows a northwest trend, resulting in northwest-trending graben. These magmatically created graben are intersected by northeast-trending normal faults that are parallel to the primary axis of the Yellowstone caldera and likely also due to hot spot activity (Christiansen 2001, Chang *et al.* 2007). These orientations may also be due to orientations of Basin and Range normal faults. Two of these NW-SE trending faults cut the caldera and movement has been detected along them using GPS measurements (Puskas *et al.* 2007).

Schroon River: The Schroon River flows through the eastern Adirondack Mountains near Elizabethtown, New York, U.S.A. The crystalline core of the Adirondack Mountains is comprised of the oldest rocks in the area and was deformed in the Proterozoic Grenville orogeny and Paleozoic Taconic orogeny (McLelland *et al.* 1996). The river features right-angle bends and straight links. This morphology is controlled by an intersecting set of NE-SW and NW-SE normal faults (Zernitz 1932, Morisawa 1985) related to orogenic compression (Quinn 1933, McLelland *et al.* 1996). According to McLelland *et al.* (1996), the normal faulting is due to delamination of overthickened crust. Quinn (1933) did not have a theory for why normal faults at multiple orientations could be related to compression, but he cited orogenic compression as the most likely explanation for the normal faults in the Adirondacks. The Adirondack Mountains may be continuing to rise tectonically, and there may be present-day movement along existing normal faults (Isachsen 1975).

Zambezi River: The Zambezi River in southern Africa flows through Zambia, the Democratic Republic of Congo, Angola, Namibia, Botswana, Zimbabwe, Mozambique, Malawi, and Tanzania. This river drains a Jurassic basaltic plateau (Zernitz 1932). It is often used as an example of rectangular drainage due to its clear right-angle bends and very straight links, particularly prominent in the reach below Victoria Falls. Twidale (2004) also noted the reach immediately downstream of Victoria Falls which follows a series of sharp, hairpin turns. The flow of the river is controlled by graben, which represent the southern-most extent of the East African Rift Zone (Vail 1968, Moore and

Larkin 2001). Rifting may be due to a mantle plume that became active 30-40 million years ago and that has caused regional uplift and crustal extension (Roberts *et al.* 2012).

Katherine River: The Katherine River has its headwaters in Nitmiluk National Park in the Northern Territory of Australia, north of the town of Katherine. The river follows fractures in the Arnhem Land Plateau which is composed of Proterozoic sandstone of the Kombolgie Subgroup (Needham and Stuart-Smith 1985, Baker and Pickup 1987) in the area of the Katherine River Gorge. The river has carved deep canyons into the plateau at right angles, exploiting NW-SE and ENE-WSW trending normal faults and joints (Needham and Stuart-Smith 1985, Sweet *et al.* 1999), as well as less resistant diabase dikes that intruded along joints in the sandstone (Needham and Stuart-Smith 1985). These normal faults formed as part of an Early Proterozoic rift system and the orientations of the faults correspond to the orientations of gravity lineaments in the area. These faults were reactivated periodically through the Mesozoic (Needham and Stuart-Smith 1985).

In these four examples, the features that control the rectangular morphology of the drainage networks are extensional, including graben (Yellowstone, Zambezi), normal faults (Yellowstone, Schroon) and fractures and joints (Katherine). However, the mechanisms for producing the tensional stress that formed these extensional features vary, including magmatism (Yellowstone, Zambezi) and rifting (Schoon, Zambezi, Katherine). There are multiple extensional events whose structures control these networks. Thus, the tectonic features that control the four rectangular rivers investigated here are uniformly extensional, although the mechanisms that produce these features are variable.

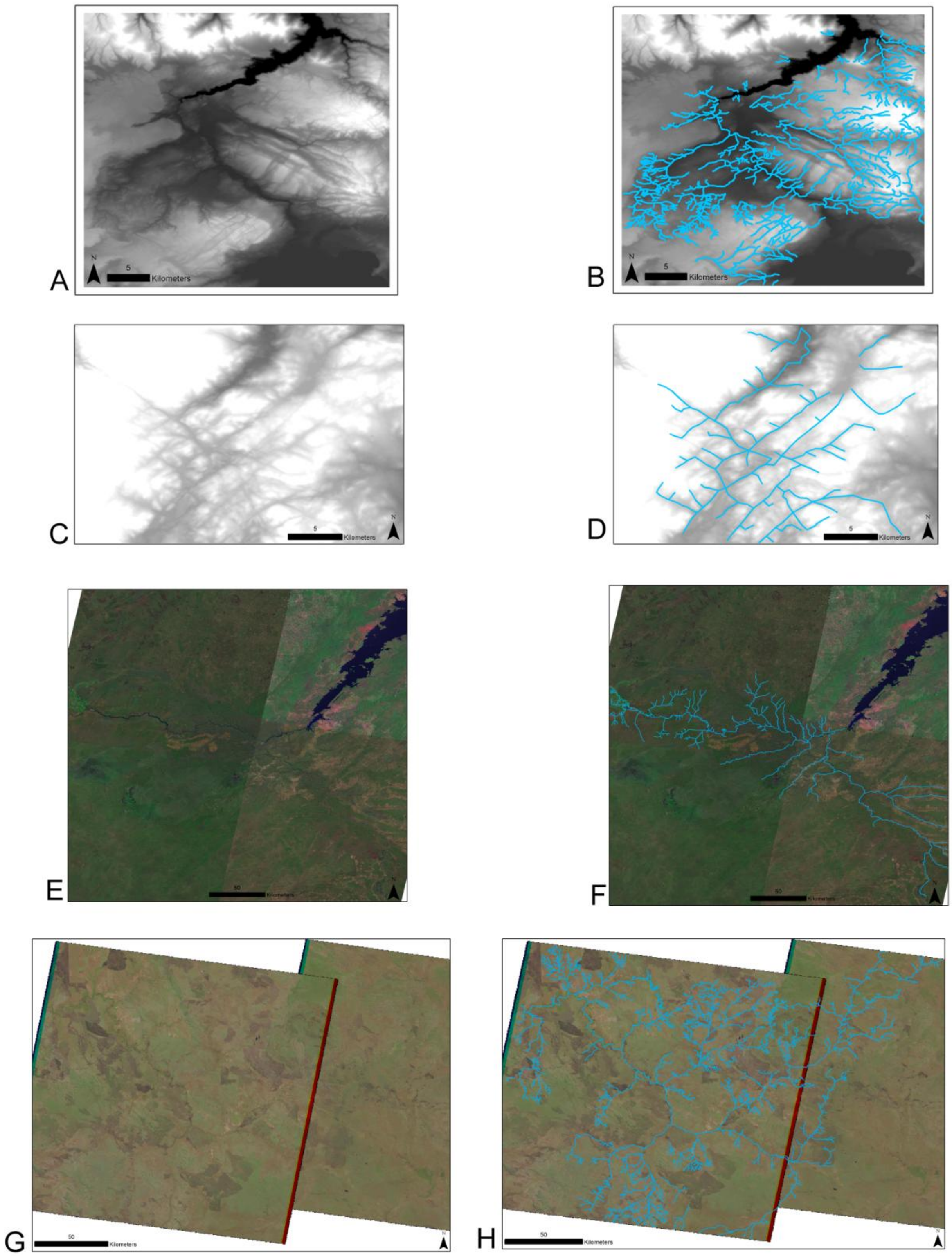
A
B
C
D
E
F
G
H
5
Kilometers
50
N

Figure 10. Terrestrial rectangular networks.

(A) Yellowstone River basin in National Elevation Dataset, (B) Yellowstone River basin in National Elevation Dataset with mapping overlain, (C) Schroon River basin in National Elevation Dataset, (D) Schroon River basin in National Elevation Dataset with mapping overlain, (E) Zambezi River basin in Landsat mosaic, (F) Zambezi River basin in Landsat mosaic with mapping overlain, (G) Katherine River basin in Landsat mosaic, (H) Katherine River basin in Landsat mosaic with mapping overlain.

V. DISCUSSION

5.1 Flow direction

Directionality of flow has previously been described for swaths through T13 (Lorenz *et al.* 2008). In Xanadu, networks located at 10°S, and spanning from 70°W to 140°W, indicate flow away from central or north Xanadu presently or when channels formed. Small networks in the northern tropics (15°N, 90°W) and mid-latitudes (52°N, 90°W) are directed east to northeast. Networks located at (60°S, 5°W) were interpreted as flowing to the south. These trends are consistent with the more global results of this study (Figure 4, black arrows).

This more complete dataset suggests that, despite the relatively subdued topography on Titan (Zebker *et al.* 2009, Lorenz *et al.* 2011), flow directions are controlled by local topography and base level effects. The large impact crater, Menrva in the northern mid-latitudes, shows a dendritic network located along the crater's southwestern rim that appears to drain into the crater, as do short, stubby networks along the eastern crater wall. In the north polar region, and at Ontario Lacus in the south polar region, flow drains into the lakes, which provide local sinks. Features straddling 60°S in T7 have been interpreted as south-flowing distributary networks (Lorenz *et al.* 2008), although the evidence for flow direction in this network appears to us to be ambiguous.

5.2 Network classification and geographic distribution

Rectangular networks comprise more than half of all networks analyzed (Figure 4). This result is in contrast to the results of morphologic classification by Langhans *et al.* (2012), who reported dendritic networks as the most numerous of their classes. Other workers have also used the term dendritic in reference to prominent networks in areas such as Xanadu (Lorenz *et al.* 2008), the north pole (Stofan *et al.* 2007, Cartwright *et al.* 2011), and the Huygens landing site (Tomasko *et al.* 2005, Soderblom *et al.* 2007a). Although drainage systems may be generically referred to as dendritic, the dendritic morphology has specific criteria and implications (Figure 2, Table 1). Analysis here shows that prominent networks at Xanadu, in the north polar region, and at the Huygens Landing site, although qualitatively referred to as dendritic in recent network classifications, have a rectangular morphology (Figure 4, 5, 7A, 7C).

The modified algorithm was run in the same sequence as the original algorithm from Ichoku and Chorowicz (1994). The network classification results of this study indicating the rectangular pattern as constituting the majority of networks may be biased due to the sequence of drainage pattern tests in the modified algorithm. The tests for rectangularity are the first encountered in the algorithm. Hence, the first drainage pattern test that is passed is the resulting pattern classification for that network. However, if the algorithm proceeds after a successful first classification, a network may be classified as multiple patterns. In 19 of the 48 SAR networks (40%), networks were able to be classified as two or three patterns *if the classification tests were applied without the order specified in the original work*. Combinations included rectangular and parallel, rectangular and dendritic, parallel and dendritic, and rectangular, parallel, and dendritic. This could be a result of the simplification of the original algorithm, which includes two additional tests between rectangular and parallel tests, and two additional tests between parallel and the first dendritic test. These additional tests, which cannot be used due to the resolution of the SAR data, may prevent networks from having multiple classifications in the original algorithm. Thus, if the order of tests in the modified algorithm was changed, the proportions of network classifications may be different, and there may be a majority of dendritic networks, as has been qualitatively observed by other workers, although the classifications of those other authors are in some cases mutually inconsistent.

In comparison to the more limited geographic distribution of other network types, the distribution of rectangular networks indicates that the controls on rectangular networks are significant across much of Titan. The finding of rectangular networks in both SAR and DISR data indicates that these controls are effective over length scales ranging from the Huygens landing site to Xanadu. Joints and/or faults at or near right angles are hypothesized to control the shape and location of rectangular networks (Zernitz 1932, Thornbury 1954, Howard 1967, Morisawa 1985, Twidale 2004). The prevalence of these networks suggests that Titan's surface is fractured and/or faulted in the areas containing rectangular networks. However, most of the fluvial features mapped were not sufficiently integrated in available data to be considered for classification analysis (Figure 4). While this apparent lack of network integration may be a function of low image resolution, fluvial networks on Titan may generally be poorly integrated, similar to Martian valley networks (Mars Channels Working Group 1983, Carr and Malin 2000).

Like rectangular networks, trellis networks also feature straight links and near-right angle bends. In the original algorithm by Ichoku and Chorowicz (1994), "rectangularity" is required for rectangular networks, and a possible attribute of trellis networks, although not required (Figure 2). The original algorithm indicates that the most important attribute for distinguishing between trellis and rectangular networks is the mean exterior link length, which is shorter for trellis than for rectangular networks. Due to the low spatial resolution of the current data available for Titan, true headwater streams cannot be discerned (as demonstrated by the non-visibility of the DISR networks in the SAR data (Soderblom *et al.* 2007a)), so cannot assess this attribute. Thus, there may be trellis networks on Titan that have been misclassified as rectangular, given current data limitations. For future investigations, the updated classification algorithm (Figure 2) includes trellis networks for use with denoised (e.g., Lucas *et al.* 2011, Lucas *et al.* 2012), higher resolution, or otherwise improved data.

To test for possible misclassifications of trellis networks as rectangular, AIRSAR data over terrestrial trellis networks were inspected and their appearance was compared to that of SAR data over rectangular networks on Titan. Terrestrial trellis networks form in areas of folded, layered sedimentary rocks of contrasting resistance and are common in the Valley and Ridge physiographic province in the eastern U.S. (Ritter *et al.*, 2002). Particularly in Pennsylvania, where large folds are responsible for the alternating valleys and ridges, trunk channels of fluvial networks flow along these alternating valleys with smaller tributaries cutting across the ridges. In AIRSAR data of the Valley and Ridge province, topography creates alternating radar-bright and radar-dark bands as the radar-facing slopes are illuminated and the opposing slopes are shadowed (Figure 10).

The area immediately surrounding each rectangular network on Titan was inspected for evidence of alternating, linear, radar-bright and radar-dark patterns indicative of valleys and ridges or large folds. Of the 27 rectangular networks, none showed a radar pattern consistent with valley and ridge topography. However, one unanalyzed network, north of Ontario Lacus, showed a radar return pattern that could be consistent with valley and ridge topography. Thus, the analysis indicates that rectangular networks still constitute over half of the networks analyzed. Limited coverage and moderate resolution, however, hides lower order tributaries, whose detection is necessary in the algorithm to classify a network as trellis. Future work with denoised data (cf., Lucas *et al.* 2011, Lucas *et al.* 2012) or data with improved resolution sufficient to resolve fingertip tributaries (cf. Barnes *et al.* 2011) could refine the results.

Figure 10. AIRSAR data over Susquehanna River basin, Pennsylvania.
Black arrow indicates direction of radar illumination. Radar-facing slopes appear bright, while the backsides of ridges appear dark in the folds. Tributaries can be seen in some places cross-cutting ridges.

Within the uneven data coverage, the clustering of the networks, as indicated by the results of the nearest neighbor analysis, suggests that fluvial activity is more pronounced in certain areas of Titan. This concentration of activity could be due to either atmospheric or surface/subsurface effects. Atmospheric patterns may produce heavier or more consistent precipitation in some latitudinal bands compared to others, as suggested by recent precipitation modeling (e.g. Schneider *et al.* 2012). Clouds have been observed over the south pole during the southern summer with hourly variation (Atreya *et al.* 2009), similar to rainstorms on Earth. Similar phenomena were observed by Turtle *et al.* (2011) at low latitudes. At the surface or in the subsurface, clustering of networks could be due to more erodible substrate, fewer competing surface processes (dunes, resurfacing by volcanism) or greater concentrations of structures, which may facilitate formation of fluvial networks. Collins *et al.* (2011) suggested that it may be easier to erode Titan's icy bedrock if it is already fractured, providing planes of weakness.

5.3 Determination of dominant azimuths

Terrestrial studies (Eyles *et al.* 1997, Sharma *et al.* 2003, Hodgkinson *et al.* 2006, Pelletier *et al.* 2009) show that the orientation of links in drainage networks closely follows the orientation of bedrock structures. Rose diagrams of rectangular networks indicate possible orientations of structures controlling the flow. In areas where dominant orientations are comparable, the orientations may therefore reflect the orientation of the regional stress field prior to or during development of fluvial networks. "Dominant azimuths" are defined as a function of cumulative link length per 5° of azimuth. For a given network, the azimuth bin with the greatest percentage of cumulative link length is designated as the dominant azimuth for that network. Dominant azimuths for networks were compared over bands of 30° of latitude. Eyles *et al.* (1997) found buried terrestrial bedrock channels and bedrock joints with orientations within 11° to have a significant regional correspondence. This approach is followed in the work, for which orientations were considered comparable if they were within 10° of the dominant azimuths of other networks in the 30° band.

In each 30° latitudinal band with rectangular networks on Titan (Table 6), there is comparability in the dominant azimuths. In some, networks share dominant azimuths; in others, the dominant azimuth of a network is within 5° or 10° of the dominant azimuth of adjacent networks. Consistent dominant azimuths suggest control by a regional stress regime and lend support to our classification methodology. Neighboring north polar networks tend not to have matching dominant azimuths, but in most of those cases, a secondary azimuth for those networks was comparable to other dominant azimuths in the area. Comparability based on secondary azimuths, however, was not investigated. The dominant azimuths globally are NE-SW, NW-SE, and to a lesser extent E-W. These azimuths are consistent with orientations of structural features identified by Paganelli *et al.* (2010), Liu *et al.* (2012), and orientations of the hypothesized faults and folds in the T43 swath as part of this work (see section 5.4 for discussion of these findings).

Because rectangular networks are indicative of structural features at approximately right angles, possible pairing of dominant azimuths in the 30° latitudinal bands was investigated to determine whether 90° pairs existed. Pairs of 80°-100° in azimuthal separation were considered to constitute right angles, following the definition by Ichoku and Chorowicz (1994).Several right-angle sets were found in the 0°S-30°S and 60°N-90°N bands. Orthogonal joint sets are rarely produced by one deformational event, however. The orthogonal surface expression may be a result of superimposed joint sets from multiple stress events or multiple sources of stress. Therefore, pairs of angle offsets common for terrestrial conjugate joint sets were sought, namely 60°/120° or less (Hatcher 1995, Hancock and Skinner 2000). 30°/150° pairs and 60°/120° pairs were found in the 0°S-30°S and 60°N-90°N bands, as well as the 30°S-60°S and 60°S-90°S bands. In half of the terrestrial examples, there are multiple stresses on the system. As explained above in section 4.6, the controlling structures for two of the four terrestrial examples-namely, the Yellowstone and Schroon Rivers-were formed through multiple deformation episodes. On Titan, timing of structures cannot be determined. If deformation on Titan is driven by processes related to its orbit, on-going deformation of Titan's ice crust would be expected. Currently the only outer solar system satellites with observed on-going endogenic processes are Io, Enceladus, and Triton. Tectonic deformation may be occurring on Titan, but it is not possible with current data to determine the timing of such activity, therefore it is assumed that all deformation is contemporaneous.

5.4 Comparison of network classification statistics

Relative to other network classifications, rectangular networks seem to have an average degree of integration, as represented by the mean Shreve magnitude. However, rectangular networks have the greatest mean network summed link length of the four classifications, indicating the greatest degree of incision. This finding supports the hypothesis of other authors (Collins *et al.* 2011) that it is easier to erode bedrock that has pre-existing weaknesses, such as fractures or faults.

Parallel networks have both the lowest mean Shreve magnitude and mean network summed link length. Low Shreve magnitudes may be expected for parallel networks due to the nature of the pattern: long tributaries flowing roughly parallel would have few junctions, thus resulting in relatively low Shreve magnitudes. However, parallel networks could have high network summed link lengths, and it is possible that the areas where parallel networks are found on Titan may be resistant to erosion, resulting in less incision and shorter links.

Because there is no set of geologic implications for unclassified networks, it is unclear why the mean Shreve magnitude is the greatest for this network classification. One explanation of unclassified networks is that the network is very large and may be subject to a variety of geologic controls. If this is the explanation for the majority of unclassified networks included in this work, the high Shreve magnitude value is easily explained.

5.5 Sources of stress for controlling structures on Titan rectangular networks

Rivers are heavily influenced by structure, whether stand-alone features such as volcanoes or impact craters, or regional structural trends. Of the eight basic drainage patterns recognized by Howard (1967), four are attributed to structures: trellis, rectangular, radial, and annular. Radial networks tend to form on the slopes of high-relief features such as volcanoes and domes. Annular networks form in depressions such as basins or impact craters or on the flanks of mature domes (Zernitz 1932, Thornbury 1954, Howard 1967, Morisawa 1985, Twidale 2004). Trellis networks form on rocks of varying resistance, often in areas of parallel folds or fractures (Zernitz 1932, Thornbury 1954, Howard 1967, Twidale 2004, Ribolini and Spagnolo 2007, Burberry et al. 2008). Rectangular networks form in areas of joints and/or faults at or near right angles (Zernitz 1932, Thornbury 1954, Howard 1967, Morisawa 1985).

While rectangular networks indicate the presence of joints or faults, they do not give any indication of the sense of movement along the faults, or what type of stress produces the joints. The drivers of tectonic stress on Earth and on Titan are different. On Earth, deformation occurs as a result of endogenic processes, the most influential being tectonic plate motion. In the outer solar system, deformation is generally associated with orbital dynamics and changes in the hydrostatic equilibrium shape of a given body. However, the stress types that could result from these different processes-tensional, compressional, or a combination to produce strike-slip features-are the same. The response of silicate rock and ice to stress is similar (Collins *et al.* 2010), and numerical modeling of a water-ice "continent" on Titan indicates that cryogenic ice would deform in a brittle manner (Perron and de Pater 2004). Thus, understanding the tectonic stresses required to produce rectangular networks on Earth should indicate the stresses required to produce equivalent features on Titan. The results of the investigation of four terrestrial rectangular networks indicate that the structures that commonly control rectangular networks (joints, fractures, normal faults, graben) form in tensional tectonic stress regimes, or in the case of the Yellowstone River, extension due to volcanism. On this basis, it is inferred that rectangular networks on Titan also form primarily in areas dominated by extension, although from different stress mechanisms.

Characteristics of rectangular networks, most notably right-angle bends, can be created by structures formed by stresses other than regional extension. Rivers that are offset across a strike-slip fault, such as Wallace Creek (Sieh and Jahns 1984) and Little Rock Creek (Morisawa 1985) along the San Andreas fault feature well-defined right-angle bends at the intersection of the river valley and fault. If unaffected outside of the fault zone, however, these rivers would likely not display the necessary proportion of right angle bends to be classified as rectangular.

Right-angle bends in drainage networks are often attributed to orthogonal joint sets (Zerntiz 1932, Thornbury 1954, Howard 1967, Morisawa 1985); however, there may be multiple ways to form orthogonal joints. There have been several mechanisms suggested for the formation of joint sets that intersect at approximately 90° angles. Caputo (1995) proposed, based on investigations of orthogonal joint sets in limestones in Great Britain, that orthogonal joint sets are due to reorientations of the principal stresses, and thus the joint sets form in cycles. Scheidegger (2001) argued that it is more logical for orthogonal joint sets to be a result of shearing as in any stress field there are always two orthogonal directions of simple shear in planview. This model is simpler in that it does not necessitate reorientation of stresses or cycles of joint formation.

Joints with right-angle intersections may also be due to superimposed joint systems, giving the appearance of orthogonality (Howard 1967, Twidale 2004). These superimposed joint systems could represent multiple episodes of deformation and/or different regional stress field orientations. Further, stresses producing mesoscale structures may be different than regional stresses. For example, Engelder (1985) described extensional cross-fold joints and fold-parallel joints in the Catskill Delta that formed in a compressive regional stress field during the Alleghanian orogeny. A similar situation is found in Zimbabwe, south of the Zambezi River, where extensional joints have propagated across an area of regional compression (Fedo *et al.* 1995). Thus, right-angle bends may form where strike-slip motion has occurred or where extensional joints form in overall compressive regimes. However, as the results of the terrestrial analysis indicate, the extensional structures that shape flow into rectangular networks are more likely to form in areas of regional extension. Therefore it is concluded that the rectangular networks on Titan are most likely to have been affected by structures formed due to tensional tectonic stress.

Evidence for extension is ubiquitous in the outer solar system and attributed to various causes (Table 7). For Europa, extensional features have been attributed to non-synchronous rotation (Helfenstein and Parmentier 1985) and diurnal tides (Kattenhorn and Marshall 2006). The tiger stripes on Enceladus may be due to nonsynchronous rotation of an ice shell over a global ocean (Patthoff and Kattenhorn 2011). Coronae on Miranda (Pappalardo *et al.* 1997) are attributed to diapirs. Grooved terrain on Ganymede is attributed to non-synchronous rotation, or a heat pulse in its interior due to differentiation (Patterson *et al.* 2010). Volume change due to phase changes in the interiors of bodies may be important on several other icy satellites (Collins *et al.* 2010 and references therein).

Table 7. Summary of stress types on outer solar system satellites.

Outer solar system satellites, stress type, corresponding tectonic features, and references.

Satellite	Type of stress	Tectonic feature(s)	Reference(s)
Europa	Tension	Troughs, normal faults, ridges, bands	Kattenhorn and Marshall 2006, Nimmo and Schenk 2006, Tufts *et al.* 2000, Schenk and McKinnon 1989
	Compression	Ridges, folds	Sullivan *et al.* 1998, Prockter and Pappalardo 2000
	Shear	Ridges, bands	Hoppa *et al.* 1999, Han and Showman 2008
Enceladus	Tension	Tiger stripes, ridges and troughs	Nimmo *et al.* 2007
	Compression	Fold and thrust belt	Helfenstein *et al.* 2006
Triton	Tension	Ridges	Prockter *et al.* 2005
	Shear	Ridges	Prockter *et al.* 2005
Ganymede	Tension	Furrows, grooved terrain	Patterson *et al.* 2010
Miranda	Tension	Coronae, normal fault scarps	Pappalardo *et al.* 1997
Ariel	Tension	Ridges and troughs	Smith *et al.* 1986
Dione	Tension	Graben, troughs	Wagner *et al.* 2006
	Compression	"Wispy terrain" faults	Moore and Schenk 2007
Rhea	Tension	"Wispy terrain" faults	Moore and Schenk 2007
Tethys	Tension	Graben	Moore and Schenk 2007
Titania	Tension	Graben, normal faults	Smith *et al.* 1986
Titan	Tension	Rectangular drainage networks	This work
	Compression	Mountains	Radebaugh *et al.* 2007, Radebaugh *et al.* 2011

Each of these stress mechanisms would produce a specific tectonic signature with zones of extension, compression, and shear over 45° bands of latitude. Collins *et al.* (2010) presented a figure showing locations of these zones for four scenarios: non-synchronous rotation, polar wander, despinning, and orbital recession (Figure 11). Nonsynchronous rotation occurs when an ice shell, decoupled from the silicate portion of the interior, rotates at a rate slightly slower than the body. The misalignment of the shell with the tidal axis creates stresses in the shell. Polar wander is a similar process to nonsynchronous rotation in that it involves separate movement of the ice shell relative to the silicate interior. Polar wander, however, occurs when the ice shell moves perpendicular to the rotation axis of the body, potentially placing the pole at the equator. Despinning occurs if a satellite is rotating more rapidly than is synchronous. The satellite's rotation will slow to become synchronous. Reducing spin rate changes the shape of the body, creating stresses at the poles and equator. Orbital recession occurs due to tidal dissipation within the planet; prograde satellites will spiral outward over time. Moving away from the planet has two effects: the tidal bulge raised on the satellite is less pronounced, and the spin rate is reduced.

Assuming that the areas where rectangular networks are found represent areas where tension is the dominant tectonic regime, Titan is not a perfect match to the predictions of any single stress mechanism (Collins *et al.* 2010 and references therein). However, these scenarios are not mutually exclusive; a combination of any of these mechanisms is possible.

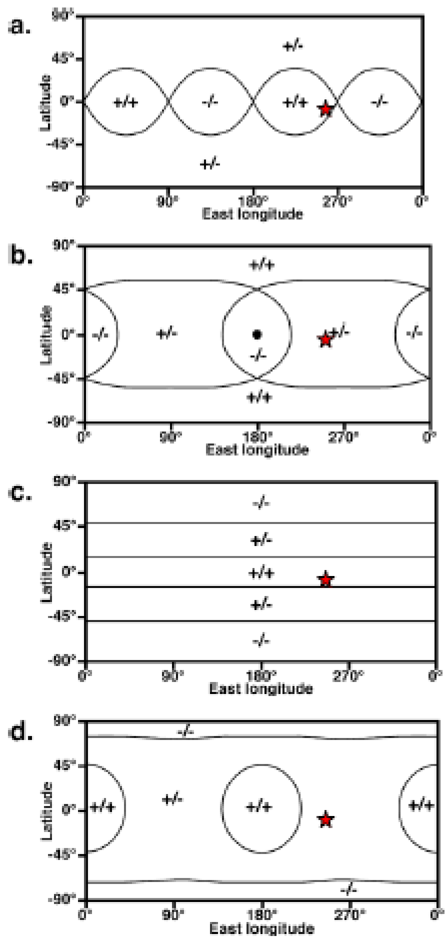

Figure 11. Tectonic modeling results.

Tectonic modeling results for (a) nonsynchronous rotation, (b) polar wander, (c) despinning, and (d) orbital recession. Modified from Collins *et al.* 2010. Red star marks approximate center of Xanadu. +/+ indicates two compressive stresses, -/- indicates two tensile stresses, +/- indicates one compressive and one tensile stress, which would likely result in strike-slip motion.

Rectangular networks are wide-spread, but the majority (67%) is found at the poles. Nine of the 27 (33%) rectangular networks from this study are located in Xanadu, but because Xanadu likely has a geologic history unique to the rest of the Titan (Radebaugh *et al.* 2011), controls on those networks are assumed to be related to this regional history and less affected by global stresses. SARTopo and RADAR altimetry data indicate that Xanadu is lower elevation than the surrounding terrain, but flow in drainage networks in Xanadu was outward as though it is a topographically high feature. Radebaugh *et al.* (2011) presented a model of Xanadu's evolution to explain the apparent discrepancy between the topographic data and observations of surface features. Radebaugh *et al.* (2011) proposed that early in Titan's history the Xanadu region experienced N-S compression, thickening the crust and creating mountains. Mountain-building was followed by NE-SW, NNW-SSE extension, creating Basin and Range-like topography and thinning the crust, creating the low topography measured at present. Although the model for the evolution of Xanadu is largely tectonic, no sources of stress are suggested. Hence the polar rectangular networks are considered as being more representative of global tectonic controls.

In view of the polar rectangular networks, non-synchronous rotation and polar wander seem less likely to have been the stress mechanisms that led to rectangular networks, as modeling results for non-synchronous rotation predict lateral strike-slip activity at the poles and results for polar wander predict compression at the poles. The modeling results for despinning and orbital recession predict tension at the poles, which is consistent with the network classification results. Liu *et al.* (2012) also suggested despinning as a likely source of stress for endogenic tectonic processes based on their analysis of equatorial mountain ranges.

Tectonic modeling results for despinning and orbital recession agree with putative structures found in Xanadu in a preliminary investigation of structures in SAR swaths. SAR swaths in Xanadu were investigated for structural features that could be related to the structurally-controlled networks due to the high density of rectangular networks. Several features are interpreted as folds and faults in the T43 radar swath at (93°W, 19°S) and (127°W, 2°S), respectively (Figure 12). The features interpreted as faults are morphologically similar to mountainous features described by Radebaugh *et al.* (2007). Both sets of features could be attributed to compression or extension. Folds are often associated with compression, and are common deformation structures in mountain chains. Folds resemble waves in that they typically consist of alternating concave-up and concave-down structures (synforms and antiforms, respectively) which form recognizable map-scale patterns (Hatcher 1995). Folds can also form due to extension-these folds are related to normal faulting, propagation of faults, and differences in displacement rate along normal faults (Schlishe 1995). While folds due to extension can be as complex as compressive folds, they are more frequently synformal, and less likely to show a typical Valley and Ridge-style fold pattern at the map scale. Due to the pattern observed near Xanadu in the T43 radar swath, these folds are interpreted as due to NW-SE compression perpendicular to the fold axes. The three semi-parallel, radar-bright features at (127°W, 2°S) are interpreted as three faults; however, due to lack of topographic data over the features, an origin is not able to be determined. These may be three thrust faults, resulting from N-S compression, or they may be three normal faults, resulting from N-S extension, creating fault block mountains. Compressive faults and folds would agree well with the model results for despinning, which predict compression in the equatorial region (Figure 11). That result would also agree with the results for orbital recession, which predicts alternating zones of compression and strike-slip motion from 45°N-45°S (Figure 12). Normal faults would not support either despinning or orbital recession.

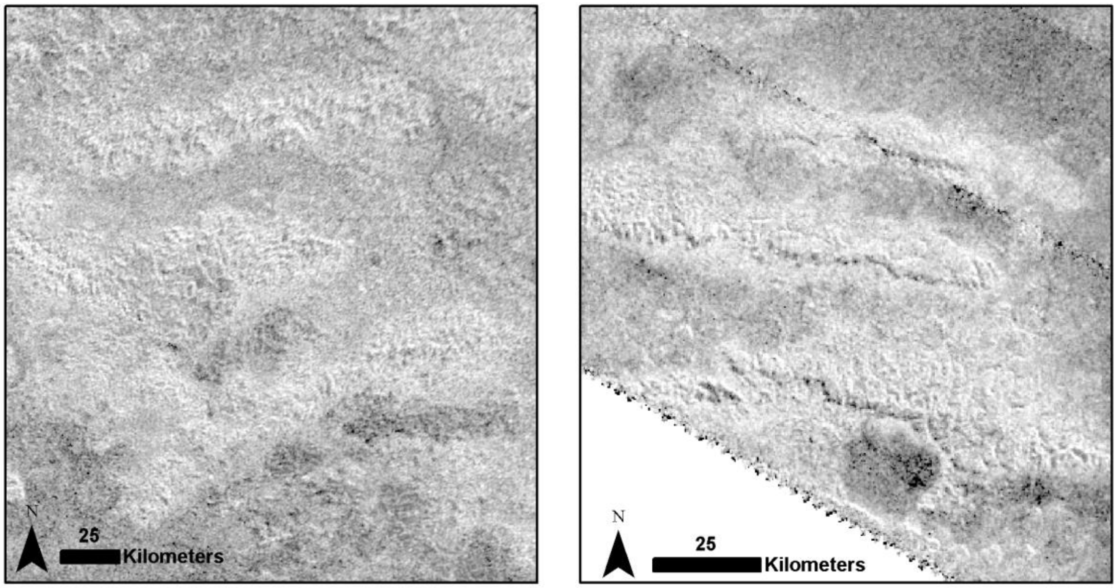

Figure 12. Folds and faults interpreted as part of this work.

The left image shows a set of folds. Image centered on (19°S, 93°W). Fold axes oriented ENE-WSW. The right image shows a set of faults. Image centered on (2°S, 127°W). Faults strike roughly WNW-ESE. In both cases, compression or extension is interpreted as perpendicular to the orientations of the structures. Both images in T43 radar swath.

If a significant number of rectangular networks are misclassified trellis networks, the geologic/tectonic implication and thus, predicted global stress mechanisms would be completely different. Trellis networks form in areas of rocks of varying resistance. Typically this situation occurs in terrain dominated by parallel folds or faults, resulting from compressional tectonics. If compression is expected in areas of trellis networks, despinning and orbital recession seem less likely stress mechanisms, as modeling results for despinning and orbital recession predict tension at the poles, while polar wander, for which compression at the poles would be expected, would seem more likely.

VI. CONCLUSIONS AND FUTURE WORK

The drainage pattern of 53 networks on Titan is analyzed, including 48 in Cassini RADAR SAR data and 5 in DISR data, and it is found that the majority are rectangular networks. The rectangular network pattern implies that network morphology is controlled by joints or faults at approximately right angles. This dominance of rectangular networks suggests that Titan's crust is globally fractured or faulted. The hypothesis that these networks are controlled by extensional structures was supported by an investigation of terrestrial rectangular networks that indicated that structures resulting from extension are common controls on rectangular river networks. Thus it is inferred that the joints and/or faults controlling rectangular networks on Titan formed due to tensional tectonic stress. Most of the rectangular networks occur in the polar regions and in Xanadu, implying that extension occurred at these locations. However, Xanadu likely has a unique geologic history, so those networks are not considered in the discussion of global stress mechanisms. The presence of rectangular networks at the poles does not correspond with tectonic modeling results for non-synchronous rotation and polar wander, which predict strike-slip motion and compression at the poles, respectively. Rather, rectangular networks at the poles appear to be more consistent with modeling results for despinning and orbital recession, which predict tension at the poles. Both of these processes, despinning and orbital recession, may be treated as single, but long-lived, deformation events. If any of these rectangular networks are misclassified trellis networks, different global stress mechanisms would be implied. Specifically, trellis networks at the poles would imply global stresses resulting from polar wander. In either case, fluvial networks of trellis or rectangular patterns indicate past or on-going tectonic activity on Titan.

Stress field on outer solar system satellites commonly vary through time as a result of orbital dynamics (Collins *et al.* 2010 and references therein).Thus it is unlikely that Titan has had a uniform stress field through time. One piece of evidence for this is the variety of orientations of rectangular network links. These varying orientations indicate a changing stress field as is expected in this work. It is unlikely that Titan's crust has remained static through time. The surface age is very young relative to other solar system bodies, which may indicate crustal regeneration. It is also unlikely that there has been only one deformation event on Titan. On Earth, right angle joints or faults are commonly due to multiple superimposed deformation events as discussed above. Thus it is unlikely that the right-angle structures on Titan are due to one deformation event. In the T43 radar swath where faults are interpreted, there are offsets in the large faults, indicating at least two events; however, these features are in Xanadu, which has been excluded from consideration of global stress due to its unique geologic history. The presence of rectangular networks clearly indicates the presence of structures on Titan; the widespread rectangular networks indicate the wide-spread nature of deformation of Titan. The comparison with terrestrial rectangular networks indicates that these controlling structures are likely extensional structures. The geophysical models against with which these results match most closely-namely despinning and orbital recession-provide a reasonable first-order stress mechanisms for the rectangular networks observed on Titan. Future modifications and refinements to these hypothesized mechanisms, e.g., consideration of variable crustal thickness and stress field orientation, will improve these results.

Future work to test the hypothesis of tectonically-induced structural control on fluvial networks on Titan, to assess the possibility that some rectangular networks may be trellis, and to classify the unclassified networks might entail multiple investigations. While higher-resolution data are desirable, testing using existing and upcoming Cassini data could be done in several ways. Mapping using denoised SAR data may be more comprehensive, including lower-order tributaries, which would result in more rigorous classifications. Upcoming Cassini SAR data may reveal more rectangular networks with regionally consistent azimuths, indicating control by a regional tectonic stress field. Comparison of orientations of rectangular network links with orientations of other tectonically-controlled features including mountain chains (Radebaugh *et al.* 2007, Liu *et al.* 2012) and unit contacts (Paganelli *et al.* 2010) may elucidate any regional structural controls. Analysis of radar backscatter in areas containing rectangular networks may also provide evidence of fractured bedrock. Higher-resolution data, such as could be collected from an airplane on Titan (Barnes *et al.* 2011) would further enable rigorous testing of the results of the drainage pattern analysis. A further test for tectonic control on fluvial networks on Titan could involve tectonic modeling of Titan, specifically, comparing modeled orientations of principal stresses with orientations of mapped features (cf. Collins 2010). Further tests for tensional tectonics could include analysis of topographic data over rectangular network drainage basins and use of higher-resolution imagery to look for offset features.

The preponderance of rectangular fluvial networks provides evidence for widespread fracturing and/or faulting of Titan's crust. Fluvial erosion exploits the fractures and faults, forming rectangular network patterns on the surface. Thus Titan's external processes reveal the presence of an internal process-tectonism. Tectonism may provide or have provided an important resurfacing mechanism, and may in part account for the young surface age of Titan. Resurfacing by tectonism allows for slower or less efficient surface processes on Titan (Black *et al.* 2012), or a recent acquisition of a thick atmosphere (Lorenz *et al.* 1997, Moore and Nimmo 2012).

REFERENCES CITED

Atreya, S.K., et al., 2009. Volatile origin and cycles: nitrogen and methane. In: Brown, R.H., Lebreton J., Waite, J.H. (Eds.), Titan from Cassini-Huygens, Springer, Dordrecht, pp.177-199.
Baker, V.R., and Pickup, G., 1987. Flood geomorphology of the Katherine Gorge, Northern Territory, Australia. GSA Bull. 98, 635-646.
Barnes, J.W., et al., 2007. Near-infrared spectral mapping of Titan’s mountains and channels. J. Geophys. Res. 112, E11006 doi:10.1029/2007JE002932.
Barnes, J.W., et al., 2008. Spectroscopy, morphometry, and photoclinometry of Titan's dunefields from Cassini/VIMS. Icarus 195, 400-414.
Barnes, J.W., et al., 2011. AVIATR—Aerial Vehicle for In-situ and Airborne Titan Reconnaissance: A Titan airplane mission concept. Exp. Astron. DOI: 10.1007/s10686011-9275-9.
Baugh, N.F., 2008. Fluvial channels on Titan. Master’s thesis. University of Arizona.
Black, B.A., Perron, J.T., Burr, D.M., Drummond, S.A., 2012. Estimating erosional exhumation on Titan from drainage network morphology. J. Geophys. Res., doi:10.1029/2012JE004085.
Brown, R.H., et al., 2004. The Cassini Visual and Infrared Mapping Spectrometer (VIMS) Investigation. Space Science Reviews 115, 111-168.
Burberry, C.M., Cosgrove, J.W., Liu, J.G., 2008. Spatial arrangement of fold types in the Zagros Simply Folded Belt, Iran, indicated by landform morphology and drainage pattern characteristics. Jour. of Maps, 417-430.
Burr, D.M., Emery, J.P., Lorenz, R.D., Collins, G.C., Carling, P.A., 2006. Sediment transport by liquid surficial flow: Application to Titan. Icarus 181, 235-242.
Burr, D.M., et al., 2009. Fluvial network analysis on Titan: Evidence for subsurface structure and west-to-east wind flow, southwestern Xanadu. Geophys. Res. Lett. 36, L22203, doi:10.1029/2009GL040909.
Burr, D.M., et al., 2012. Fluvial features on Titan., GSA Bull., in revision.
Burt, J.E., Barber, G.M., Rigby, D.L., 2009. Elementary Statistics for Geographers. Guilford Press. New York.
Caputo, R., 1995. Evolution of orthogonal joint sets of coeval extension joints. Terra Nova 7, 479-490.
Carr, M.H., and Malin, M.C., 2000. Meter-scale characteristics of Martian channels and valleys. Icarus 146, 366-386.
Cartwright, R., Clayton, J.A., Kirk, R.L., 2011. Channel morphometry, sediment transport, and implications for tectonic activity and surficial ages of Titan basins. Icarus 214, 561-570.
Chang, W., Smith, R.B., Wicks, C., Farrell, J.M., Puskas, C.M., 2007. Accelerated Uplift and Magmatic Intrusion of the Yellowstone Caldera, 2004 to 2006. Science 318, 952-956.
Christiansen, R.L., 2001. The Quaternary and Pliocene Yellowstone Plateau Volcanic Field of Wyoming, Idaho, and Montana. USGS Professional Paper 729-G.
Collins, G.C., 2005. Relative rates of fluvial bedrock incision on Titan and Earth. Geophys. Res. Lett. 32, L22202, doi:10.1029/2005GL024551.

Collins, G.C., 2010. Testing candidate driving forces for faulting on Dione: implications for nonsynchronous rotation and a freezing ocean. American Geophysical Union Fall Meeting 2010, P24A-08.
Collins, G.C., et al., 2010. Tectonics of the Outer Planet Satellites. In: Watters, T.D. and Schultz, R.A. (Eds.), Planetary Tectonics, Cambridge University Press, Cambridge, pp. 264-350.
Collins, G.C., Polito, P.J., Litwin, K.L., Sklar, L.S., 2011. Resistance of water ice to fluvial abrasion and implications for erosion on Titan. 42nd Lunar Planet. Sci. Conf., 2781.
Drummond, S.A., Burr, D.M., Cartwright, R., Black, B.A., Perron, J.T., 2011. Global mapping and morphologic classification of Titan fluvial features. 42nd Lunar Planet. Sci. Conf., 1919.
Elachi, C., et al., 2005. Cassini Radar views the surface of Titan. Science 308, 970-974.
Engelder, T., 1985. Loading paths to joint propagation during a tectonic cycle: example from the Appalachian Plateau, U.S.A. J. of Struct. Geology 7, 459-476.
Eyles, N., Arnaud, E., Scheidegger, A.E., Eyles, C.H., 1997. Bedrock jointing and geomorphology in southwestern Ontario, Canada: an example of tectonic predesign. Geomorphology 19, 17-34.
Fedo, C.M, Eriksson, K.A., Blenkinsop, T.G., 1995. Geologic history of the Archean Buhwa Greenstone Belt and surrounding granite - gneiss terrane, Zimbabwe, with implications for the evolution of the Limpopo Belt. Can. J. Earth Sci. 32, 1977 1990.
Griffith, C., Hall, J., Geballe, T., 2000. Detection of daily clouds on Titan. Science 290, 509-513.
Hancock, P.L. and Skinner, B.J., eds., 2000. The Oxford Companion to the Earth. Oxford University Press. Oxford. 1184 p.
Hatcher, R.D., Jr., 1994. Structural geology: principles, concepts, and problems. Prentice Hall, Englewood Cliffs, NJ. 528 p.
Hayes, A., et al., 2010. Hydrocarbon lakes on Titan: Distribution and interaction with a porous regolith. Geophys. Res. Lett. 35, L09204, doi:10.1029/2008GL033409.
Hayes, A.G., et al., 2011. Transient surface liquid in Titan's polar regions from Cassini. Icarus 211, 655-671.
Helfenstein, P., and Parmentier, E.M., 1985. Patterns of fracture and tidal stresses on Europa. Icarus 53, 415-430.
Helfenstein, P., et al., 2006. Patterns of fracture and tectonic convergence near the south pole of Enceladus. Lunar Planet. Sci. 37, 2182.
Howard, A. D., 1967. Drainage analysis in geologic interpretation: A summation. AAPG Bull. 51, 2246–2259.
Hynek, B.M., and Phillips, R.J., 2003. New data reveal mature, integrated drainage systems on Mars indicative of past precipitation. Geology 31 (9), 757-760.
Ichoku, C. and Chorowicz, J., 1994. A numerical approach to the analysis and classification of channel network patterns. Water Resour. Res. 30(2), 161-174.
Isachsen, Y.W., 1975. Possible evidence for contemporary doming of the Adirondack Mountains, New York, and suggested implications for regional tectonics and seismicity. Tectonophysics 29, 169-181.

Jaumann, R., et al., 2008. Fluvial erosion and post-erosional processes on Titan. Icarus 197, 526-538.
Jaumann, R., et al., 2009. Geology and Surface Processes on Titan. In: Brown, R.H., Lebreton J., Waite, J.H. (Eds.), Titan from Cassini-Huygens, Springer, Dordrecht, pp.75-140.
Kattenhorn, S.A. and Marshall, S.T., 2006. Fault-induced perturbed stress fields and associated tensile and compressive deformation at fault tips in the ice shell of Europa: Implications for fault mechanics. J. Struct. Geol. 28, 2204-2221.
Kirk, R.L., et al., 2005. Radar reveals Titan topography. 36th Lunar Planet. Sci. Conf., 2227.
Kirk, R.L., Howington-Kraus, E., Stiles, B.W., Hensley, S., Cassini RADAR team, 2008. Digital topographic models of Titan produced by radar stereogrammetry with a rigorous sensor model. 39th Lunar Planet. Sci. Conf., 2320.
Kirk, R.L., et al., 2010. La Sotra y las otras: Topographic evidence for (and against) cryovolcanism on Titan. American Geophysical Union Fall Meeting, 2010, P22A 03.
Knighton, D., 1998. Fluvial forms and processes: a new perspective. Arnold, London. 383 p.
Lamb, M.P., Howard, A.D., Johnson, J., Whipple, K.X., Dietrich, W.E., Perron, J.T., 2006. Can springs cut canyons into rock?. J. Geophys. Res. 111, E07002, doi:10.1029/2005JE002663.
Lamb, M., Dietrich, W., Aciego, S., DePaolo, D., and Manga, M., 2008, Formation of Box Canyon, Idaho, by megaflood: Implications for seepage erosion on Earth and Mars. Science 320, 1067-1070.
Langhans, M.H., et al., 2012. Titan's fluvial valleys: Morphology, distribution, and spectral properties. Planet. Space Sci. 60 (1), 34-51.
LeGall, A., Janssen, M.A., Paillou, P., Lorenz, R.D., Wall, S.D., the Cassini Radar Team, 2010. Radar-bright channels on Titan. Icarus 207, 948-958.
Leopold, L.B., Wolman, M.G., Miller, J.P., 1964. Fluvial Processes in Geomorphology. Freeman, San Francisco. 522 p.
Liu, Z.Y.C., et al., 2012. Evidence for an endogenic origin of mountains on Titan. 43rd Lunar Planet. Sci. Conf., 2378.
Lopes, R.M.C., et al., 2007, Cryovolcanic features on Titan's surface as revealed by the Cassini Titan Radar Mapper. Icarus 186, 395-412.
Lopes, R.M.C., et al., 2010. Distribution and interplay of geologic processes on Titan from Cassini radar data. Icarus 205, 540-558.
Lopes, R.M.C., et al., 2011. Cryovolcanism on Titan: a re-assessment in light of new data from Cassini RADAR and VIMS. EPSC-DPS Joint Meeting, 2011.
Lorenz, R.D., McKay, C.P., Lunine, J.I., 1997. Photochemically drive collapse of Titan's atmosphere. Science 275, 642-644.
Lorenz, R.D., et al., 2007. Titan's young surface: Initial crater survey by Cassini RADAR and model comparison. Geophys. Res. Lett. 34, L07204. doi:10.1029/2006GL028971.
Lorenz, R. D., et al., 2008. Fluvial channels on Titan: Initial Cassini RADAR observations. Planet. Space Sci. 56, 1132-1144.

Lorenz, R.D., et al., 2011. Hypsometry of Titan. Icarus 211, 699-706.
Lucas, A., Aharonson, O., Hayes, A.G., Deledalle, C.A., Kirk, R.L., 2011. Enhanced processing and analysis of Cassini SAR images of Titan. American Geophysical Union Fall Meeting 2011, P33E-1795.
Lucas, A., et al., 2012. Clues to Titan hydrology from enhanced SAR image processing. 43rd Lunar Planet. Sci. Conf., 2566.
Lunine, J.I. and Atreya, S.K., 2008. The methane cycle on Titan. Nature Geoscience 1, 159-164.
Mars Channels Working Group, 1983. Channels and valleys on Mars. GSA Bull. 94, 1035-1054.
Mitri, G., Showman, A.P., Lunine, J.I., Lorenz, R.D., 2007. Hydrocarbon lakes on Titan. Icarus (186), 385-394.
Mejía, A.I. and Niemann, J.D., 2008. Identification and characterization of dendritic, parallel, pinnate, rectangular, and trellis networks based on deviations from planform self similarity. J. Geophys. Res. 113, F02015, doi:10.1029/2007JF000781.
Moore, A.E., and Larkin, P.A., 2001. Drainage evolution in south-central Africa since the breakup of Gondwana. S. Afr. J. Geol. 104, 47-68.
Moore, J.M., and Nimmo, F., 2012. Does Titan's landscape betray the late acquisition of its current atmosphere? 43rd Lunar Planet. Sci. Conf., 1248.
Moore, J.M., and Pappalardo, R.T., 2011. Titan: An exogenic world?. Icarus 212, 790 806.
Moore, J.M., and Schenk, P., 2007. Topography of endogenic features on Saturnian midsized satellites. Lunar Planet. Sci. 38, 2136.
Morisawa, M., 1985. Rivers: form and process. Longman, London. 222 p.
Needham, R.S., and Stuart-Smith, P.G., 1985. Stratigraphy and tectonics of the Early to Middle Proterozoic transition, Katherine-El-Sherana area, Northern Territory. Australian Jour. Earth Sciences 32, 219-230.
Neish, C.D., and Lorenz, R.D., 2012. Titan's global crater population: a new assessment. Planet. Space Sci. 60, 26-33.
Nimmo, F., and Pappalardo, R.T., 2006. Diapir-induced reorientation of Saturn's moon Enceladus. Nature 441, 614-616.
Nimmo, F. and Schenk, P., 2006. Normal faulting on Europa: Implications for ice shell properties. J. Struct. Geol. 28, 2194-2203.
Paganelli, F., et al., 2010. Preliminary analysis of structural elements of Titan and implications for stress. 41st Lunar Planet. Sci. Conf., 2664.
Patthoff, D. A., and Kattenhorn, S. A., 2011. A fracture history on Enceladus provides evidence for a global ocean.38, L18201.
Pelletier, J.D., et al., 2009. Tectonic and structural control of fluvial channel morphology in metamorphic core complexes: The example of the Catalina-Rincon core complex, Arizona. Geosphere 5, 363-384.
Perron, J.T. and de Pater, I., 2004. Dynamics of an ice continent on Titan. Geophys. Res. Lett. 31, L17S04, doi:10.1029/2004GL019802.

Perron, J.T., Lamb, M.P., Koven, C.D., Fung, I.Y., Yager, E., Adámkovics, M., 2006. Valley formation on Titan. J. Geophys. Res. 111, E11001, doi:10.1029/2005JE002602.
Porco, C. C., et al., 2005. Imaging of Titan from the Cassini spacecraft. Nature 434, 159 168.
Prockter, L.M., and Pappalardo, R.T., 2000. Folds on Europa: Implications for crustal recycling and accommodation of extension. Science 289, 941-944.
Prockter, L.M., Nimmo, F., Pappalardo, R.T., 2005. A shear heating origin for ridges on Triton. Geophys. Res. Lett. 32, L14202.
Puskas, C. M., Smith, R.B., Meertens, C.M.,Chang, W.L., 2007, Crustal deformation of the Yellowstone–Snake River Plain volcano-tectonic system: Campaign and continuous GPS observations, 1987–2004, J. Geophys. Res., 112, B03401, doi:10.1029/2006JB004325.
Radebaugh, J., et al., 2007. Mountains on Titan observed by Cassini Radar. Icarus 192, 77-91.
Radebaugh, J., et al., 2008. Dunes on Titan observed by Cassini Radar. Icarus 194, 690 703.
Radebaugh, J., et al., 2011. Regional geomorphology and history of Titan's Xanadu province. Icarus 211, 672-685.
Ribolini, A., and Spagnolo, M., 2007. Drainage network geometry versus tectonics in the Argentera Massif (French–Italian Alps). Geomorphology 93, 253-266.
Ritter, D.F., Kochel, R.C., Miller, J.R., 2002. Process Geomorphology. Waveland Press, Long Grove, IL. 560 p.
Roberts, E. M., et al., 2012, Initiation of the western branch of the East African Rift coeval with the eastern branch: Nature Geosci, v. 5, no. 4, p. 289-294,
Scheidegger, A.E., 2001. Surface joint systems, tectonic stresses and geomorphology: a reconciliation of conflicting observations. Geomorphology 38, 213-219.
Schenk, P., and Jackson, M.P.A., 1993. Diapirism on Triton: A record of crustal layering and instability. Geology 21, 299-302.
Schlishe, R.W., 1995. Geometry and origin of fault-related folds in extensional settings. AAPG Bull. 79, 1661-1678.
Schneider, T., Graves, S.D.B., Schaller, E.L., Brown, M.E., 2012. Polar methane accumulation and rainstorms on Titan from simulations of the methane cycle. Nature Let. doi:10.1038/nature10666.
Sharma, B.K., Bhola, A.M., Scheidegger, A.E., 2003. Neotectonic activity in the Chamba Nappe of the Himachal Himalaya: jointing control of the drainage patterns. J. Geol. Soc. India 61, 159-169.
Sieh, K.E., and Jahns, R.H., 1984. Holocene activity of the San Andreas fault at Wallace Creek, California. GSA Bull. 95, 883-896.
Smith, B.A., et al., 1986. Voyager 2 at Neptune: Imaging science results. Science 246, 1422-1449.
Soderblom, L.A., et al., 2007a. Topography and geomorphology of the Huygens landing site on Titan. Planet. Space Sci. 55, 2015-2024.

Soderblom, L.A., et al., 2007b. Correlations between Cassini VIMS spectra and RADAR SAR images: Implications for Titan's surface composition and the character of the Huygens Probe Landing Site. Planet. Space Sci. 55, 2025-2036.
Sotin, C., et al., 2005. Release of volatiles from a possible cryovolcano from near infrared imaging of Titan. Nature 435, 786-789.
Stiles, B.W., et al., 2009. Determining Titan surface topography from Cassini SAR data. Icarus 202 (2), 584-598.
Stofan, E.R., et al., 2007. The lakes of Titan. Nature 445 (4), 61-64.
Sullivan, R., et al., 1998. Episodic plate separation and fracture infill on the surface of Europa. Nature 391, 371-373.
Sweet, I.P., Brakel, A.T., and Carson, L., 1999, The Kombolgie Subgroup-a new look at an old "formation": Australian Geological Survey Organization Research Newsletter 30, 26–28.
Thornbury, W.D., 1954. Principles of geomorphology. Wiley, New York, 594 p.
Thornbury, W.D., 1965. Regional geomorphology of the United States. Wiley, New York. 602 p.
Tomasko, M. G., et al., 2005. Rain, winds and haze during the Huygens probe's descent to Titan's surface. Nature 438 (8), doi: 10.1038/nature04126.
Tufts, B.R., Greenberg, R., Hoppa, G., Geissler, P., 1999. Astypalaea Linea: A large scale strike-slip fault on Europa. Icarus 141, 53-64.
Tufts, B.R., Greenberg, R., Hoppa, G., Geissler, P., 2000. Lithospheric dilation on Europa. Icarus 146, 75-97.
Turtle, E.P., et al., 2009. Cassini imaging of Titan's high-latitude lakes, clouds, and south-polar surface changes. Geophys. Res. Lett. 36, L02204 doi:10.1029/2008GL036186.
Turtle E.P., Perry, J.E., Hayes, A.G., McEwen, A.S., 2011. Shoreline retreat at Titan's Ontario Lacus and Arrakis Plantitia from Cassini Imaging Science subsystem observations. Icarus 212, 957-959.
Turtle, E.P., et al., 2011. Rapid and extensive surface changes near Titan's equator: Evidence of April showers. Science 331, 1414-1417.
Twidale, C.R., 2004. River patterns and their meaning. Earth Sci. Rev. 67, 159-218.
Vail, J.R., 1968. The southern extension of the East African Rift System and related igneous activity. Geologische Rundschau 57 (2), 601-614.
Wall, S.D., et al., 2009. Cassini RADAR images at Hotei Arcus and western Xanadu, Titan: Evidence for geologically recent cryovolcanic activity. Geophys. Res. Lett. 36, L04203, doi:10.1029/2008GL036415.
Wall, S., et al., 2010. Active shoreline of Ontario Lacus, Titan: A morphological study of the lake and its surroundings. Geophys. Res. Lett. 37, L05202, doi:10.1029/2009GL041821.
Wasiak, F.C., Androes, D., Blackburn, D.G., Chevrier, V., Dixon, J., 2012. Characterization of Ligeia Mare in the north polar region of Titan. 43rd Lunar Planet. Sci. Conf., 1720.
Welivitya, W.D.D.P., Wasiak, F., Tullis, J.A., Blackburn, D.G., Chevrier, V., 2012. A remote sensing and GIS approach for change detection on Titan's lakes using Cassini orbiter's SAR data. 43rd Lunar Planet. Sci. Conf., 1678.

Wood, C.A., Lorenz, R., Kirk, R., Lopes, R., Mitchell, K., Stofan, E., Cassini RADAR Team, 2010. Impact craters on Titan. Icarus 206, 334–344. doi:10.1016/j.icarus.2009.08.021.

Zebker, H.A., Stiles, B., Hensley, S., Lorenz, R., Kirk, R.L., Lunine, J., 2009. Size and shape of Saturn's moon Titan. Science 324, 921-923.

Zernitz, E. R., 1932. Drainage patterns and their significance. Jour. Geology 40, 498-521.

VITA

Sarah A. Drummond was born August 7, 1987. She is the daughter of Garry and Dana Drummond and has a younger brother, Ned. She calls the Eastern Shore of Virginia home and grew up outside of a small town called Parksley.

Sarah attended elementary through high school at Broadwater Academy in Exmore, Virginia. At Broadwater, Sarah was valedictorian, a class officer throughout high school, and member of the Beta Club, Tri-Hi-Y, Chorale, and Battle of the Brains team. She attended Model General Assembly sophomore-senior year, served as a committee chairman, and was selected to attend the National Young Leaders Conference. She attended educational summer programs at the Virginia Spaceflight Academy and Presidential Classroom. From third grade through twelfth grade she danced at the Eastern Shore's Own Arts Center School of Ballet and spent summers dancing at the Richmond Ballet.

Sarah received a BS cum laude in Environmental Sciences with a minor in Astronomy at the University of Virginia in Charlottesville, Virginia. She did two years of undergraduate research on fluvial geomorphology on Mars with Prof. Alan Howard and used her research to complete the department's Distinguished Majors Program. Sarah danced with the University Dance Club, Rhapsody Ballet Ensemble, Monroe-Highland Scottish Country Dancers, and took Irish dancing classes through the Blue Ridge Irish Music School. She worked as a Resident Advisor for first-year students for two years, volunteered with the Rivanna Trails Foundation, and is a member of Alpha Delta Pi sorority.

During her master's degree, Sarah has been an active member of the department Geology Club, and served as vice-president and president of that organization. She has volunteered at the McClung museum for three years and volunteered with Earth Science Fair and Science Olympiad events.